isvr Institute of Sound and Vibration Research

The One-Dimensional Bubble: Theory, Experiment, and Relevance to Exposure of Divers to Low Frequency Sound, and of Lung to Lithotripsy

T.G. Leighton, P.R. White and M.A. Marsden

ISVR Technical Report No 246

May 1995

University of Southampton

SCIENTIFIC PUBLICATIONS BY THE ISVR

Technical Reports are published to promote timely dissemination of research results by ISVR personnel. This medium permits more detailed presentation than is usually acceptable for scientific journals. Responsibility for both the content and any opinions expressed rests entirely with the author(s).

Technical Memoranda are produced to enable the early or preliminary release of information by ISVR personnel where such release is deemed to the appropriate. Information contained in these memoranda may be incomplete, or form part of a continuing programme; this should be borne in mind when using or quoting from these documents.

Contract Reports are produced to record the results of scientific work carried out for sponsors, under contract. The ISVR treats these reports as confidential to sponsors and does not make them available for general circulation. Individual sponsors may, however, authorize subsequent release of the material.

COPYRIGHT NOTICE

(c) ISVR University of Southampton All rights reserved.

ISVR authorises you to view and download the Materials at this Web site ("Site") only for your personal, non-commercial use. This authorization is not a transfer of title in the Materials and copies of the Materials and is subject to the following restrictions: 1) you must retain, on all copies of the Materials downloaded, all copyright and other proprietary notices contained in the Materials; 2) you may not modify the Materials in any way or reproduce or publicly display, perform, or distribute or otherwise use them for any public or commercial purpose; and 3) you must not transfer the Materials to any other person unless you give them notice of, and they agree to accept, the obligations arising under these terms and conditions of use. You agree to abide by all additional restrictions displayed on the Site as it may be updated from time to time. This Site, including all Materials, is protected by worldwide copyright laws and treaty provisions. You agree to comply with all copyright laws worldwide in your use of this Site and to prevent any unauthorised copying of the Materials.

UNIVERSITY OF SOUTHAMPTON

INSTITUTE OF SOUND AND VIBRATION RESEARCH

FLUID DYNAMICS AND ACOUSTICS GROUP

The one-dimensional bubble: Theory, Experiment, and relevance to exposure of divers to low frequency sound, and of lung to lithotripsy

by

T G Leighton, P R White and M A Marsden

ISVR Technical Report No. 246

May 1995

Approved: Professor J K Hammond
Director, ISVR

© Institute of Sound & Vibration Research

CONTENTS

FIGURE CAPTIONS

Figure 1 Schematic of 1-D bubble

Figure 2 Plot of stiffness as a function of displacement for air bubble in water. Predictions in both the adiabatic ($\kappa=\gamma=1.4$) and isothermal ($\kappa=1$) limits are shown. Those from the nonlinear theory (i.e. from equation 25) are solid lines. The small amplitude approximate form (equation 26), which would predict linear oscillations, are broken lines.

Figure 3a Plots of the effect of bubble length, shown as a proportion of tube which is filled by air at equilibrium, on the natural frequency, as predicted by linear theory in the limit of small-amplitude oscillations. The solid lines indicate calculations for which the inertia of the fluid in the cone is neglected, and the dashed line corresponds to calculations including the inertia of the fluid in the cone. The upper two plots correspond to the adiabatic ($\kappa=\gamma$) case, and the lower two to the isothermal ($\kappa=1$) situation. Viscous effects are neglected.

Figure 3b Plots of the effect of tube length on the natural frequency, for the adiabatic ($\kappa=\gamma$, broken lines) and isothermal ($\kappa=1$, solid lines) cases. Results are shown for tubes filled at equilibrium by gas to a proportion (from the top) of 2%, 5%, 10% and, for the lowest lines, 50%. Tube diameter is assumed to be small compared to tube length, but surface tension and viscous effects are neglected.

Figure 4 Solutions of equation 33 give phase space plots of bubble wall velocity as a function of wall displacement for the free undamped oscillation of a bubble having $\omega_0/2\pi$ = 23 Hz. The normalised initial displacement increases from (a)-(d): (a) 0.05, (b) 0.10, (c) 0.25, (d) 0.35.

Figure 5 The displacement time histories associated with the solutions shown in the corresponding parts of figure 4.

Figure 6 The frequency spectra associated with the displacement time histories shown in the corresponding parts of figure 5.

Figure 7 The apparatus employed to measure the phase response of a driven bubble.

Figure 8 The phase response of the driven bubble. Experimental measurements at discrete frequencies are joined by solid line. The numerical solutions are shown for the adiabatic ($\kappa=\gamma$) and isothermal ($\kappa=1$) cases, as the labels show. Solutions to the inviscid equation of motion (equation 28) are shown as long dashes (__ __ __). Solutions to the equation of motion incorporating viscous effects (equation 38) as shown as short dashes (- - - -).

Figure 9a The amplitude response of the driven bubble. Experimental measurements at discrete frequencies are joined by solid line. The numerical solutions are shown for the adiabatic ($\kappa=\gamma$) and isothermal ($\kappa=1$) cases, as the labels show. Solutions to the inviscid equation of motion (equation 28) are shown as long dashes (__ __ __). Solutions to the equation of motion incorporating viscous effects (equation 38) as shown as short dashes (- - - -).

Figure 9b The acceleration of the vibrator which gave the response shown in 9a.

Figure 10 Resonance of air bubbles in ear canals as a function of ambient pressure (and equivalently, depth) for a 2.5 cm ear canal of diameter 5 mm filled to (a) 50% (solid line ____), and (b) 10% (dashed __ __ __) and (c) 2% (dotted line _ _ _ _) operating in a piston-like manner (equation 38). Viscosity is incorporated, but the inertia of the liquid outside the canal is neglected (justified since the filling of air is to less than 50%). Values of 1000 kg/m^3 and 9.8 m/s^2 are assumed for the water density and acceleration due to gravity, respectively.

ABSTRACT

In this paper the oscillation dynamics of a linear gas pocket in a liquid are analysed. These include several features of potential use at undergraduate level for illustrating characteristics beyond those normally encountered in expositions of simple harmonic oscillators (for example, the simple linear spring-bob system). The oscillator in question is unusual firstly in that, as with all gas bubbles in liquid, the inertia is invested primarily in the surrounding liquid, rather than in the pocket itself. In other words the radiation mass is far larger than the mass of the trapped gas. This is demonstrable even in the simplest analysis, that of linear undamped small-amplitude oscillations. Secondly, the oscillator is nonlinear. The equation of motion of a damped, forced, one-dimensional bubble is obtained, the nonlinearity arising through the dependence of the oscillator stiffness (or alternatively the gas compressibility) on the amplitude of oscillation. In reduced forms, this equation can be solved analytically for the natural frequency of undamped oscillations in the linear limit, and also in the nonlinear regime of finite-amplitude free oscillation, where the fundamental frequency is found to be amplitude-dependent. Whilst analytical solutions of the undamped, unforced form of the equation of motion can be obtained in phase space, the full nonlinear damped forced equation must be solved numerically. These solutions are compared with those of the linear undamped analysis. Experimental measurements of the phase and amplitude response of a laboratory one-dimensional bubble are made, and compared with theory. Viscous effects, which for three dimensional bubbles in water are second-order and often justifiably neglected in simple analyses based on the gas stiffness and liquid inertia, are in the case of one-dimensional water bubbles comparable with these other effects (*i.e.* stiffness and inertia), and cannot be neglected. The analysis is used to predict (i) the response of air bubbles within the ear canals of divers to low frequency underwater sound (from several tens of hertz to several hundred, such as is being used increasingly in the ocean for climate monitoring), and (ii) the theoretical potential of bubbles in blood to cause haemorrhage of blood vessels, particularly within the lung, when subjected to high-amplitude ultrasonic pulses.

INTRODUCTION

Most students are introduced to the physics of oscillators through the behaviour of an idealised mass-spring system. If the bob of mass m undergoes a displacement ε, the spring (assumed to be massless) responds by applying a force of $-k\varepsilon$. If there is a damping force proportional to the speed of the bob, then the equation governing the motion of the bob is found from Newton's Second Law to be

$$m\ddot{\varepsilon} + b\dot{\varepsilon} + k\varepsilon = F \qquad (1)$$

where F represents any external forces applied to drive the system. In the absence of a driving force and damping, substitution of the linear solution $\varepsilon=\varepsilon_o\cos\omega_o t$ into equation 1 shows that the disturbed system undergoes oscillation at the natural circular frequency ω_o, where

$$\omega_o = \sqrt{k/m} \quad , \qquad (2)$$

and so is independent of ε_o, the amplitude of the displacement. Equation 2 can also be obtained by equating the maximum kinetic energy of the system, $\Phi_{K,max}$, which is attained when the bob passes through the equilibrium position ($\varepsilon=0$; $|\dot{\varepsilon}| = \omega_o\varepsilon_o$), with the maximum potential energy that is stored in the system, $\Phi_{P,max}$. The potential energy stored in the spring reaches a maximum at either extreme of the motion ($\varepsilon=\varepsilon_o$; $|\dot{\varepsilon}| = 0$) such that

$$\Phi_{P,max} = \int_0^{\varepsilon_o} k\varepsilon \, d\varepsilon = \frac{1}{2} k\varepsilon_o^2 . \qquad (3)$$

Equating this to

$$\Phi_{K,max} = \frac{1}{2} m(\omega_o\varepsilon_o)^2 , \qquad (4)$$

yields equation 2, the natural frequency of the undamped oscillator.

In conditions of light damping (i.e. when $b^2<4km$), substitution of the trial solution $\varepsilon=Ae^{st}$ into equation 1 yields $s=- b/2m \pm i\omega_b$, where $i^2=-1$, such that the motion is a damped oscillation of the form

$$\varepsilon = (\Xi_1 e^{i\omega bt} + \Xi_2 e^{-i\omega bt})\, e^{-(b/2m)t} \quad \text{, or equivalently} \tag{5}$$

$$\varepsilon = (X_1 \sin\omega_b t + X_2 \cos\omega_b t)\, e^{-(b/2m)t}\,, \tag{6}$$

where $\Xi_{1,2}$ and $X_{1,2}$ are constants indicating the amplitude of oscillation; and where the frequency of oscillation,

$$\omega_b = \sqrt{(4km - b^2)} \;\; / 2m\,, \tag{7}$$

is less than ω_o, the natural frequency of the undamped motion, by an amount which increases with the damping (French, 1979).

This idealised system is sufficient to illustrate how the ratio of the two primary characteristics of the oscillator, stiffness and inertia (represented in the idealised spring/bob model by k and m respectively) relate to the natural frequency for undamped motion; and how damping reduces the frequency of oscillation.

The idealised model outlined above differs from the real spring/bob oscillator in both the stiffness and the inertia. Such features may be introduced into an increasingly involved model. Whilst at small amplitudes the stiffness is independent of the displacement, at larger amplitude this is not the case. The spring may for example be extended beyond its elastic limit, and the motion becomes history-dependent. Whilst the inertia in the simple model is invested wholly in the bob, in reality a displacement of the bob will cause a displacement of component elements of the spring, and a driving force will not only have to accelerate the bob but also the material of the spring. However, there is inertia invested elsewhere, in addition to the bob and the spring. When the bob is displaced upwards, a volume of air must be displaced downwards: the driver must provide not only the kinetic energy of the bob, and that of the varying elements of the spring (which move with velocity roughly in proportion to distance from a fixed point) but also the kinetic energy of an amount of the surrounding gas.

The inertial contribution from the surrounding fluid is characterised by the so-called "radiation mass" m_r, which is defined through $\Phi_{KE,max}$, the maximum kinetic energy of the surrounding *fluid* only, in the following way:

$$\Phi_{KE,max} = \tfrac{1}{2} \;\; m_r \; |\dot{\varepsilon}_{\;max}|^2 \tag{8}$$

(compare with equation 4).

In the one-dimensional bubble, these departures from the ideal spring-bob oscillator are accentuated. Whilst in the spring/bob oscillator the radiation mass is generally negligible in comparison with the inertia of the bob, when gas is trapped in bubbles in liquid, the inertia associated with acceleration of the relatively dense liquid is very much greater than the inertia of the gas itself.

In addition, the stiffness (which as with all gas bubbles in liquids is provided by the compressibility of the gas) is dependent on the displacement. Whilst the nonlinear oscillations of three-dimensional bubbles has been studied for some time (Leighton, 1994), less is known of one-dimensional bubbles, which may feature significantly in the interaction with sound of gas pockets within several biological structures.

THEORY

Natural frequency of the undamped bubble (small amplitude harmonic motion assumed)

The natural frequency of the undamped one dimensional bubble can be calculated by equating the maximum potential energy with the maximum kinetic energy, as was done for the idealised spring/bob model in equations 2 to 4. Initially, surface tension, friction and viscous effects are ignored, as are the possibilities of meniscus deformation.

Potential energy of the gas

The idealised one-dimensional bubble analysed here and shown in figure 1, is modelled as a cylindrical pocket of gas contained within rigid walls except at the flat interface with the liquid, which can move only in a piston-like manner. The liquid is contained within the rigid walls of a connected tube and cone. The liquid is assumed to be incompressible, and all the potential energy is taken to be invested within the compressibility of the gas. Assume that the gas within the bubble behaves polytropically, such that

$$pV^{\kappa} = \text{constant}, \tag{9}$$

where p is the gas pressure within the bubble, of volume V, and where κ is the so-called polytropic index (which varies between γ, the ratio of the specific heat of the gas at constant pressure to that at constant volume, and unity, depending on whether the gas is behaving adiabatically, isothermally, or in some intermediate manner). Therefore

the gas pressure and bubble volume at equilibrium (p_o, V_o) can be related to values at some general position through

$$\frac{p}{p_o} = \left(\frac{V_o}{V}\right)^{\kappa} = \left(\frac{A_o x_o}{A_o x_o - A_o \varepsilon}\right)^{\kappa} , \tag{10}$$

where A_o is the cross-sectional area of the bubble, ε the displacement of the meniscus from equilibrium (positive for the upwards direction), and x_o the bubble length at equilibrium (see figure 1). If $\varepsilon \ll x_o$ then equation 10 can be expanded to give the change in gas pressure from equilibrium to be

$$p - p_o = \frac{\kappa \varepsilon p_o}{x_o} . \tag{11}$$

If an incremental displacement $d\varepsilon$ occurs, and the bubble volume changes by $dV = A_o d\varepsilon$, then the incremental change in the potential energy of the gas is

$$d\Phi_{PE} = -(p - p_o)dV. \tag{12}$$

Integrating equation 12 from equilibrium to the extreme of the oscillation, using substitution from equation 11, gives the maximum potential energy stored in the gas

$$\Phi_{PE,max} = \int_0^{\varepsilon_o} \frac{\kappa A_o p_o}{x_o} \varepsilon d\varepsilon = \left(\frac{\kappa A_o p_o}{x_o}\right)\frac{\varepsilon_o^2}{2} . \tag{13}$$

Kinetic energy of the liquid

The inertia of the gas is assumed to be negligible, owing to the much greater density (ρ) of the liquid. Assume a harmonic displacement ε of the meniscus, $\varepsilon = \varepsilon_o e^{i\omega_o t}$. Since the liquid is assumed to be incompressible, the maximum kinetic energy of the liquid in the column (of equilibrium length $y_o = H_1 - x_o$), of mass $\rho A_o y_o$, occurs when the speed is a maximum (i.e. $|\dot{\varepsilon}_{max}| = \omega_o \varepsilon_o$) and the displacement zero, and equals

$$\Phi_{KE,max,col} = \tfrac{1}{2} \rho A_o y_o \omega_o^2 \varepsilon_o^2 . \tag{14}$$

Since the cross-sectional area in the cone increases with distance from the meniscus, so that the flow velocity of the incompressible liquid decreases in proportion, the area (A), radius (r) and distance from the imaginary apex of the cone (h) of a horizontal section through the cone are related to their values at the base of the column (A_o, r_o, and h_o respectively -see figure 1) through

$$\frac{A_o}{A} = \frac{\pi r_o^2}{\pi r^2} = \frac{\pi(h_o \tan\theta)^2}{\pi(h \tan\theta)^2} = \frac{A_o}{\pi(h \tan\theta)^2} \quad . \tag{15}$$

where θ is the half-angle of the cone. The volume of liquid crossing all such areas A in a time dt must be constant if the liquid is incompressible, so that equating liquid fluxes gives the liquid velocity crossing the area A in the cone to be $\dot{\varepsilon}\ A_o/A$. The volume of a liquid element of thickness dh of cross-sectional area A in the cone is $\pi(h\tan\theta)^2 dh$; its mass is $\rho\pi(h \tan\theta)^2 dh$; and its maximum kinetic energy is

$$\tfrac{1}{2}\ \rho\pi(h \tan\theta)^2 dh\ |\dot{\varepsilon}_{max}|^2 (A_o/A)^2.$$

Substituting for A_o/A from equation 15, letting $|\dot{\varepsilon}_{max}|$ equal $\omega_o\varepsilon_o$, and integrating up the kinetic energy of all the liquid elements in the cone gives the maximum kinetic energy of the liquid in the cone:

$$\Phi_{KE,max,cone} = \int_{h_o}^{H_2} \left(\tfrac{1}{2}\rho\pi(h \tan\theta)^2 |\dot{\varepsilon}_{max}|^2 \left(\frac{A_o}{\pi(h \tan\theta)^2}\right)^2 \right) dh$$

$$= \frac{1}{2}\frac{\rho(A_o\varepsilon_o\omega_o)^2}{\pi \tan^2\theta} \int_{h_o}^{H_2} \frac{dh}{h^2}$$

$$= \frac{1}{2}\frac{\rho(A_o\varepsilon_o\omega_o)^2}{\pi \tan^2\theta}\left(\frac{1}{h_o} - \frac{1}{H_2}\right) \quad . \tag{16}$$

The total maximum kinetic energy of the incompressible liquid is therefore

$$\Phi_{KE,max} = \Phi_{KE,max,col} + \Phi_{KE,max,cone} \ , \tag{17}$$

which can be found by substituting from equations 14 and 16 to give:

$$\Phi_{KE,max} = \frac{1}{2}\ \rho(\varepsilon_o\omega_o)^2 A_o\left(y_o + \frac{A_o}{\pi \tan^2\theta}\left(\frac{1}{h_o} - \frac{1}{H_2}\right)\right) \quad . \tag{18}$$

The natural frequency of the undamped oscillator is found, as before, by equating $\Phi_{KE,max}$ to $\Phi_{PE,max}$, which can be done through equations 13 and 18 to give

$$\omega_o = \sqrt{\frac{\kappa p_o}{\rho x_o\left(y_o + \frac{A_o}{\pi \tan^2\theta}\left(\frac{1}{h_o} - \frac{1}{H_2}\right)\right)}}$$

$$= \sqrt{\frac{\kappa p_o}{\rho x_o\left((H_1 - x_o) + \frac{A_o}{\pi \tan^2\theta}\left(\frac{1}{h_o} - \frac{1}{H_2}\right)\right)}} \quad , \tag{19}$$

which is related to the linear natural frequency, f_o, through $\omega_o = 2\pi f_o$.

The inertia

The radiation mass of this one-dimensional bubble can readily be found through comparison of equations 8 and 18 (using $|\dot{\varepsilon}_{max}| = \omega_o\varepsilon_o$), to give

$$m_r = \rho A_o y_o\left(1 + \frac{A_o}{y_o \pi \tan^2\theta}\left(\frac{1}{h_o} - \frac{1}{H_2}\right)\right) \quad . \tag{20}$$

The first term in brackets (unity) arises from the kinetic energy of the liquid in the column. Unless the volume of liquid in the column is very small (see the discussion after figure 2), then this first term has a much greater contribution to the radiation mass than the second term (typically 100 times with the experimental apparatus described later), which reflects the kinetic energy of the liquid in the cone. This is because whilst the liquid in the column has the same velocity as the meniscus, the liquid velocity in the cone falls off rapidly with depth (in the ratio A_o/A, i.e. as h^{-2}, as discussed after equation 15). As a result the radiation mass of such a bubble is only slightly greater (typically 1% more) than the mass of liquid in the column, $\rho A_o y_o$, but very much less than the actual gravitational mass of liquid, which equals

$$\rho A_o y_o\left(1 + \frac{\pi \tan^2\theta}{3A_o y_o}\left(H_2^3 - h_o^3\right)\right) \quad . \tag{21}$$

In equation 21, the first term (unity) represents the gravitational mass of the liquid in the column, and the second term (which for this apparatus is roughly two orders of magnitude larger) represents the gravitational mass of the liquid in the cone.

The stiffness

Having obtained the effective inertia of the oscillator, an expression for the stiffness, if available, has two uses. Firstly the ratio of the stiffness to the inertia can be used to obtain the natural frequency (and so provide a check on the earlier expression), as in equation 2; and secondly it can be used to formulate the equation of motion of the oscillator (see equation 1). In this case it also serves to illustrate a source of nonlinearity.

As outlined in the introduction, the stiffness k of this oscillator can be found by determining the force exerted by the bubble in response to a displacement ε. That force can be characterised through the change in gas pressure p, so that

$$k = A_o \frac{\partial p}{\partial \varepsilon} \quad . \tag{22}$$

The term $\partial p/\partial \varepsilon$ can readily be calculated from equation 10, recalling that $A_o x_o = V_o$:

$$\frac{\partial p}{\partial \varepsilon} = \kappa A_o p_o V_o^{\kappa} (V_o - A_o \varepsilon)^{-(\kappa+1)} \tag{23}$$

which can be simplified to

$$\frac{\partial p}{\partial \varepsilon} = \frac{\kappa A_o p_o}{V_o} \left(1 - \frac{\varepsilon}{x_o}\right)^{-(\kappa+1)} . \tag{24}$$

Substitution of this into equation 22 gives the stiffness of the bubble to be:

$$k = \frac{\kappa p_o A_o^2}{V_o} \left(1 - \frac{A_o \varepsilon}{V_o}\right)^{-(\kappa+1)} . \tag{25}$$

This is seen to deviate from the stiffness of the ideal spring/bob system in that it is not constant, but instead is dependent on the displacement, and so will vary throughout the oscillatory cycle. Figure 2 plots the stiffness of the gas for both positive and negative values of meniscus displacement ε. The nonlinear expression for stiffness, equation 25,

is plotted as solid curves for both the adiabatic and isothermal limits. As can be seen from figure 2, the stiffness increases in compression ($\varepsilon>0$), and decreases in rarefaction. If the change in volume is so small as to be negligible compared to the equilibrium bubble volume (i.e. $A_o|\varepsilon|\ll V_o$) then the stiffness becomes independent of displacement, and of value

$$k = \frac{\kappa p_o A_o^2}{V_o} \quad . \tag{26}$$

This small-amplitude approximation is also indicated on figure 2 as dashed lines corresponding to the isothermal and adiabatic limits, in which the stiffness is indeed constant through an oscillatory cycle, and so would correspond to a linear oscillation. Following equation 2, the root of the ratio of the small-amplitude approximation to the stiffness (as given by equation 26) to the radiation mass (from equation 20) gives the natural frequency of the undamped oscillator, in agreement with equation 19. If, for the radiation mass, the inertia of the liquid in the column only is used, and the effect of the liquid in the cone is neglected, the following approximation to the natural frequency is obtained:

$$\omega_o = \sqrt{\frac{\kappa p_o}{\rho x_o y_o}}$$

$$= \sqrt{\frac{\kappa p_o}{\rho x_o (H_1 - x_o)}} \quad . \tag{27}$$

This is equivalent to neglecting the kinetic energy of the liquid in the cone, $\Phi_{KE,max,cone}$, in the derivation given in equations 9 to 19, and instead of equation 17 applying in its place $\Phi_{KE,max} \approx \Phi_{KE,max,col}$. Within this approximation the natural frequency, as given by equation 27, is symmetrical about the midpoint of the column as regards the equilibrium position of the meniscus, the term $x_o y_o = x_o(H_1 - x_o)$ reaching a maximum when $x_o = y_o = H_1/2$, at which point the natural frequency as given by equation 27 becomes a minimum. The term $x_o y_o$ is zero when either x_o or y_o are zero (i.e. there is either no liquid, or no gas, within the column) at which point the resonance frequency becomes undefined.

The effect of bubble length within a tube of given length on the natural frequency is shown in figure 3a. The solid lines correspond to the approximation where the inertia of liquid in the cone is neglected, and the dashed lines to when it is not. In both cases the frequencies predicted by adiabatic theory are greater than those predicted by

isothermal theory, the discrepancy being significantly more than that caused by neglecting the cone mass except when the tube is nearly full of gas (equivalence occurs at around 90% filling). In agreement with equation 27, the solid plots from linear theory in the limit of small-amplitude oscillations, neglecting the mass of the fluid within the cone predict (i) that a tube which is ψ% air-filled will have the same natural frequency as a tube which is (100-ψ)% air-filled, and (ii) that this frequency becomes undefined for the conditions of $x_0=0$ (no bubble present) and $x_0=H_1$ (air fills tube completely). Whilst the first scenario need not be considered, in the second clearly the inertia of the fluid outside the tube is important in establishing a physically meaningful oscillation. Indeed it can be seen that when the inertia of the fluid within the cone is considered, the plot of equation 19 departs from that of equation 27 to give a finite natural frequency for the $x_0=H_1$ condition.

The natural frequencies of tubes of various lengths which are filled by bubbles to 50%, 10%, 5% and 2% are shown in figure 3b, using equation 27. The smaller the proportion of tube filled (for cases that are ≤50%), the higher the natural frequency for a given tube length. The dashed lines correspond to the adiabatic condition, and below each is the solid line corresponding to the isothermal oscillation with the same proportion of tube filled. The inertia of the liquid outside the tube is assumed to have negligible effect for tubes long in comparison with the bubble length and the tube diameter. The other inherent approximations (small-amplitude displacements, with negligible damping, viscous and surface tension effects, and no meniscus deformation) are still maintained. Equation 19 (and its reduction, equation 27) both employ an inherent assumption that the stiffness is independent of the displacement. Since the stiffness has in fact been shown to be displacement-dependent (equation 25), the actual response of the oscillator may only be found by formulating the equation of motion, in analogy with equation 1.

The equation of motion

This can be found through substitution of the radiation mass, as given by equation 20, and the stiffness, as given by equation 25, for the appropriate terms in equation 1. The assumptions are still that the liquid is incompressible, and that the inertia of the gas is negligible. A damping term may also be included.

$$m_r\ddot{\varepsilon} + b\dot{\varepsilon} + k\varepsilon = F \quad \Rightarrow$$

$$\left(\rho A_o y_o\left(1 + \frac{A_o}{y_o \pi \tan^2\theta}\left(\frac{1}{h_o} - \frac{1}{H_2}\right)\right)\right)\ddot{\varepsilon} + b\dot{\varepsilon} + \frac{\kappa p_o A_o^2}{V_o}\left(1-\frac{A_o\varepsilon}{V_o}\right)^{-(\kappa+1)}\varepsilon = F$$

(28)

The motion can be analysed by presenting the undamped, unforced version of equation 28, explicitly

$$\left(\rho A_o y_o \left(1 + \frac{A_o}{y_o \pi \tan^2\theta} \left(\frac{1}{h_o} - \frac{1}{H_2} \right) \right) \right) \ddot{\varepsilon} + \frac{\kappa p_o A_o^2}{V_o} \left(1 - \frac{A_o \varepsilon}{V_o} \right)^{-(\kappa+1)} \varepsilon = 0 \tag{29}$$

which can be more compactly expressed in terms of the normalised displacement $x=\varepsilon/x_o$ as

$$\ddot{x} + \omega_o^2 (1-x)^{-(\kappa+1)} x = 0 \tag{30}$$

where the constant ω_o^2 is defined by the formulation of equation 19. Note that whilst the notation ω_o^2 imitates the classical notation for the linear equation describing simple harmonic motion, in this nonlinear equation however it only reflects the natural frequency for small displacements. Equation 30 can be solved in phase space by making the substitution

$$\ddot{x} = v\frac{dv}{dx} \qquad \text{where } v=\dot{x} \tag{31}$$

to give the separable first order differential equation

$$v\frac{dv}{dx} = - \omega_o^2 (1-x)^{-(\kappa+1)} x \tag{32}$$

Integration of both sides of this equation yields

$$\left.\begin{aligned} v = \frac{dx}{dt} &= \omega_o \sqrt{\frac{2(1-\kappa x)}{\kappa(\kappa-1)(1-x)^{\kappa}} + c} \qquad (\kappa \neq 1) \\ v = \frac{dx}{dt} &= \omega_o \sqrt{\frac{2}{(1-x)} - \ln(1-x) + c} \qquad (\kappa = 1) \end{aligned}\right\} \tag{33}$$

where c is an arbitrary constant. This equation relates displacement to velocity, that is, it is a solution in phase space. Further integration will be required to obtain

displacement as an explicit function of time, a task best suited to numerical rather than analytical methods. However the solution of equation 33 does enable the description of a trajectory of the solution in phase space.

Figure 4 illustrates four typical trajectories obtained from equation 33 for the free undamped oscillations of a bubble having $\omega_o/2\pi$ = 23 Hz with four different initial displacements. The closed form of these curves indicates the periodic nature of the solutions. The curves are not of the ellipsoidal form that the linear model would produce, a difference which increases with increasing initial displacement, indicating significant departures from linearity in these solutions.

Using numerical integration the time histories associated with the solutions shown in the corresponding parts of figure 4 can be calculated (figure 5). The corresponding frequency content of these solutions is shown in figure 6. At small initial displacements the oscillation is nearly sinusoidal (figure 5a), with a fundamental frequency of 23 Hz (figure 6a), in accordance with the natural resonance predicted by the small-amplitude linear theory through equation 19. However for the larger initial displacements the greater the harmonic content of the frequency content (figure 6), as reflected in the increasing asymmetry of the time histories in figure 5. This arises because, in compression, the system has an increasing stiffness and therefore a more rapid response; conversely, in rarefaction, the stiffness is reduced and the response more sluggish, in agreement with figure 2. The fundamental frequency, as given by the peak closest to the origin in each spectrum in figure 6, decreases with increasing displacement, being (a) 23 Hz, (b) 23 Hz, (c) 21 Hz, and (d) 18 Hz.

The analytical treatment of the equations of motion which are either damped, forced, or both, is not feasible, and requires the adoption of the numerical path. The solution to equation 30 can be calculated using standard Runge-Kutta algorithms (Forsythe *et al.* 1977). A sinusoidal form for the forcing term is assumed. The size of the damping term can be obtained from theory, and has been solved for similar geometries, though the analysis is not simple (Miller and Nyborg, 1983; Miller and Neppiras, 1985). In this case estimates of the quality factor were obtained from experimental data (see later), and a value of Q=3.5 was chosen.

EXPERIMENTAL

An experimental one-dimensional model bubble was constructed within the laboratory in order to investigate the limitations of this theory. The bubble model uses glass capillary tubing of ≈123 mm length (depending on exact position of screw top), having

an internal diameter of 1.5 mm and a wall thickness of about 2 mm, attached to an inverted glass funnel. The base of this funnel is covered with a rubber diaphragm (figure 7), which is connected by bolt to a vibrator. Because of the area ratio of the funnel mouth to the diameter of the capillary tube, a small displacement of the diaphragm will produce a displacement approximately twenty times greater in the tube, so facilitating observation of the meniscus motion and minimising vibration of the glassware. The glassware has two stopcocks attached at either end of the capillary to enable both the control of pressure and the introduction of a known amount of liquid (which was degassed, filtered, and coloured with food dye).

The diaphragm is driven by a Ling vibrator (type 409) supplied by a sinusoidal signal, the excitation frequency and amplitude being made adjustable by the sinewave generator (Therlby Thandor type TG220) and amplifier. The acceleration is measured using an accelerometer connected via a charge amplifier (Bruel and Kjaer types 4367 and 2635 respectively) to a storage oscilloscope (Gould type OS1420).

Two types of measurements were made, each requiring a different set of equipment. The phase sensor comprised a photoresistor (NORP-12) and an LED which was masked to minimise light transmission through paths other than those which crossed the tube interior, such that the obscuration of the light by the dyed water produced a signal which, when incorporated into the circuit shown in figure 7, could be used to monitor the meniscus displacement. The driver (accelerometer) and response (photoresistor) signals were displayed on the oscilloscope as an X-Y plot, in the resulting Lissajous figures. These could then be interpreted to give the driver-response phase relationship, once all the phase changes introduced by the electronics had been accounted for (including filter effects). The light detector signal was filtered to reduce mains interference using a low pass filter (Barr and Stroud type EF3-04) set to 50 Hz. Since the accelerometer signal tended to be corrupted by noise, particularly at low frequencies and at low amplitudes, a 40 Hz low-pass filter (Fern Developments type EF5-02) was incorporated. The phase response for increasing frequencies was found for constant acceleration amplitude. Although adequate for the measurement of phase, this procedure proved to be inadequate for demonstrating an amplitude resonance. This was due to the fact that a constant amplitude voltage input signal to the vibrator, for increasing frequency, resulted in an increasing acceleration amplitude generated by the driver: hence to keep the acceleration amplitude constant (as monitored with the accelerometer), the input voltage to the vibrator has to be reduced each time the frequency is increased. This process decreases the displacement amplitude of the meniscus to such an extent that the optics used to measure displacements were not sensitive enough to detect a resonance peak. This problem was overcome by taking

displacement measurements for constant input voltage to the driver as the frequency varied, the acceleration amplitude of the vibrator being continually recorded. The amplitude of displacement was found by illuminating the moving meniscus with a stroboscope (Dawe type 1204C) tuned to a frequency approximately twice that of the driver. This optically reduced the velocity of the image of the meniscus, so that the extreme of the oscillation could be measured using a travelling microscope (Type 2162-HB) with a Vernier scale.

RESULTS

Measurements of phase relationship between the driver and a one-dimensional bubble oscillator (x_0=71.5±0.5 mm, y_0= 52.0±0.5 mm), taken from the accelerometer and photoresistor signals respectively and suitably corrected for phase changes in the electronics, are shown as a function of frequency in figure 8. The acceleration amplitude of the vibrator was constant at 8.92 m/s^2. The amplitude response of another bubble (x_0=70.0±0.5 mm, y_0= 53.0±0.5 mm) is shown in figure 9a, the driver amplitude (which, as explained above, necessarily increased with frequency) is shown in figure 9b. Taken at discrete frequencies, experimental results, joined by a solid line, are shown with the associated error. The experimental parameters are summarised in Table 1. The table also lists the resonance frequencies, as determined from these experimental data, and as calculated through the various theories. The analysis presented so far follows the classical formulation for spherical bubbles presented by Minnaert (1933), and as such neglects viscous effects. It gives rise to equation 28, integration of which in the limits of κ=1 and κ=γ yields the broken curves (i.e. long dashes labelled "inviscid" in figures 8 and 9a). The resonances predicted by this theory, which allows for finite amplitude nonlinear damped oscillations and employs the experimentally-determined quality factor of 3.5, are shown in Table 1. Also shown are the natural frequencies predicted by the infinitesimal-amplitude inviscid linear theory (equation 19). For the calculations, p_0= 10^5 Pa and ρ=1000 kg m^{-3}.

Fig	x_o/mm	y_o/mm	Vibrator acceleration amplitude /($s^{-2}m$)	Resonance (Linear theory, eqn. 19) / (Hz)	Resonance (Numerical theory eqn. 28) / (Hz)	Resonance (Experimental) / (Hz)
8	71.5±0.5	52.0±0.5	8.92	26.1±0.2 (κ=1) 30.9±0.2 (κ=1.4)	26.0±0.5 (κ=1) 31.0±0.5 (κ=1.4)	26±1
9a	70.0±0.5	53.0±0.5	Fig. 9b	26.1±0.2 (κ=1) 30.9±0.2 (κ=1.4)	25±1 (κ=1) 30.0±0.5 (κ=1.4)	26±2

Table 1 Comparison of experiment with inviscid theories : linear (equation 19) and numerical (equation 28).

DISCUSSION

Estimations of the resonance frequency by linear theory tend to be greater than the experimental results. As a result the isothermal approximation gives better agreement. However experience with three-dimensional bubbles leads us to expect that bubbles of such relatively large sizes as those tested experimentally should tend closer to the adiabatic, not the isothermal, case (Devin 1959). The theories expounded in the preceding sections differ from the physical one dimensional bubble in several key aspects. Though viscous damping is by far the least important mechanism in bubbles as large as a few millimetres (compared to energy losses associated with acoustic radiation and thermal processes (Devin, 1959)), the geometry of the one-dimensional bubble is very different, and suggests that the effect of viscosity must be considered.

Additional assumptions in the theory include that of uniform acceleration over the diaphragm (which it clearly is not since for the experimental bubble the perimeter is fixed) and that surface tension can be neglected. Whilst deformations of the meniscus have been neglected, such deformations are however readily observable in the experimental bubble, and are of an oscillatory nature. The presence of a second oscillator in the system may clearly have important implications to the dynamics.

The dynamics of similar oscillators have been studied in the past. Howkins (1965) made observations and preliminary calculations regarding the oscillations of gas bubbles in water attached to the submerged base of an inverted vibrator (both roughly

spherical bubbles beneath a plane face, and gas pockets trapped within 'pits' within the base). Analyses have been made of several other cases. Miller (1979) studied cylindrical bubbles bounded by elastic walls, to model the response to ultrasound of gas spaces of micron-order size between plant cells within *Elodea*. The cylindrical bubbles within this model were assumed to vibrate in the radial mode, rather than be dominated by motion of the end-walls, and the stiffness of the plant walls was very much dominant over the stiffness of the gas. Other analyses include the diaphragm-like oscillation of the meniscus as it undergoes a Bessel-function deformation, the so-called 'clamped-drumhead' vibration. This was first considered for a small circular meniscus within a solid plane (i.e. having infinitesimal thickness, but infinite in the other two dimensions) separating two half-spaces, one of gas and the other, liquid (Miller, 1979). The oscillator was therefore baffled, as were two later geometries in which this membrane was placed. These two geometries both incorporate a gas pocket which fully fills a space within a submerged solid sheet (Miller and Nyborg, 1983). In the first case, the space consists of a perforation right through the sheet, and in the second, a uniform circular pit in the surface of the sheet. In all these cases the resonance frequency and the damping were found. The 'clamped-drumhead' resonance of a meniscus within a partially-filled perforation and pit within a flat solid sheet was also found. This case represented a departure from the earlier ones, in that the inertia was not solely invested in the liquid outside the hole, but also included that due to the liquid in the hole. Miller and Nyborg (1983) also examined the piston-like motion of the bubble wall, as discussed in this paper, but only for the baffled case, where the gas fully fills the pore. This constraint was relaxed somewhat by Miller and Neppiras (1985), who discussed the oscillations of a partially-filled pore within a flat solid sheet in terms of two distinct regimes, those of 'clamped-drumhead', and of piston-like, motion. At small amplitudes, symmetrical perforations gave the same resonances as pits which had the same depth and gas content as half of a perforation.

Miller and Nyborg (1983) show that for such pore geometries, if the thickness Λ of the viscous boundary layer is an appreciable fraction of the radius of the cylinder, r_o, then the effective inertia of the liquid content of the cylinder is increased by a factor $(1+\Lambda/r_o)$. The boundary layer thickness is given by $\Lambda=\sqrt{(\mu/\pi\rho f_p)}$, where μ is the liquid viscosity and f_p the linear resonance frequency of the piston-like mode resembling the one discussed in this paper. The value of Λ for the experimental bubble investigated in this study is around 10^{-4} m, such that the $\sqrt{(1+\Lambda/r_o)}$ gives a correction factor to the denominator of around 8%. Owing to the low resonance frequencies that manifest in the experimental bubble, this factor is significantly larger than the 0.5% increase in denominator that would result from using the radiation mass as opposed to simply using the mass of liquid in the column (equation 20). Incorporating the

correction for viscosity into the theoretical estimations for the resonances in Table 1 allows a much better comparison between theory and experiment (Table 2). As can be seen from the table, the resonance predicted by linear analysis incorporating viscosity, i.e.

$$\omega_0 = 2\pi f_0 = \sqrt{\frac{\kappa p_0}{\rho x_0 y_0 (1+\Lambda/r_0)}} \tag{34}$$

more closely agrees with experiment. However in those cases where agreement is outside the allowed range given by experimental error and the $1 \le \kappa \le \gamma$ range, simple theory still tends to overestimate. The numerical predictions, based now not on solutions to equation 28 but on solutions to the following equation (where the effects of viscosity on the inertia of the cylindrical liquid element are incorporated):

$$m_r \ddot{\varepsilon} + b\dot{\varepsilon} + k\varepsilon = F \quad \Rightarrow$$

$$\left(\rho A_0 y_0 \left((1+\Lambda/r_0) + \frac{A_0}{y_0 \pi \tan^2\theta}\left(\frac{1}{h_0} - \frac{1}{H_2}\right)\right)\right)\ddot{\varepsilon}$$

$$+ b\dot{\varepsilon} + \frac{\kappa p_0 A_0^2}{V_0}\left(1-\frac{A_0\varepsilon}{V_0}\right)^{-(\kappa+1)} \varepsilon = F \tag{35}$$

are plotted on figures 8, and 9a as broken curves (short dashes, labelled "With viscosity"), in the limits of $\kappa=1$ and $\kappa=\gamma$. A calculated value of $\Lambda=0.111$ mm is used in the calculations. The predicted resonances are incorporated into Table 2, and give results within experimental error of the measured values.

Fig	Resonance (Hz) Linear (equation 34)	Resonance (Hz) Numerical (equation 35)	Resonance (Hz) Experimental
8	24.1±0.2 (κ=1) 28.8±0.2 (κ=1.4)	25.0±0.5 (κ=1) 30.0±0.5 (κ=1.4)	26±1
9a	24.4±0.2 (κ=1) 28.8±0.2 (κ=1.4)	24.0±0.5 (κ=1) 29±1 (κ=1.4)	26±2

Table 2 Comparison of the experimentally-determined resonances with those determined by theories which incorporate viscous effects (linear analysis and numerical solutions). Values for x_0, y_0 and the acceleration are as shown in Table 1.

The importance of this analysis and calculation lie not in their ability to predict the behaviour of a laboratory experimental bubble: attempts to construct even a rudimentary one-dimensional bubble resulted in a device too complicated to allow exact agreement with theory. The one-dimensional bubbles of real interest exist in biological structures, and two of these in particular are exposed to intense sound of a particular frequency. The first case is of one-dimensional bubbles trapped within ear canals of divers, and the adverse effects on divers and other mammals exposed to high intensity sound in the marine environment is currently of great concern. The second case is of one dimensional bubbles trapped within capillary blood vessels. This may occur particularly in the lung, and evidence suggests that the lowest thresholds for damage by clinical ultrasound in mammals *in vivo* are found in the lung.

Given that the biological consequences of the excitation of such gas bodies may be very important, and given in addition the preliminary indications that mammalian lung and ears are particularly sensitive to very high and very low frequency sound respectively, the importance of these calculations is to suggest whether they predict that such gas bodies, under such conditions, may indeed respond in a significant manner. For such purposes the degree of agreement between idealised theory and the simplest model available (which even so is still too complex to allow exact modelling by theory) is adequate.

Divers today are increasingly becoming exposed to high-intensity sound in the underwater environment both as unwanted noise from apparatus associated with their work, and from the increasingly common acoustic techniques associated with communication, exploration, monitoring, and exploitation of the oceans by man. Apparatus may include tools operated by the divers themselves (including stud guns, plasma cutters, rock drills, jet cleaning tools, impact wrenches, grinders and drills) which may produce sound pressure levels (SPL) of 150-170 dB (re 20 μPa) underwater, up to 210 dB SPL (re 20 μPa) having been recorded (Molvaer and Gjestland, 1981; Nedwell *et al.*, 1993). Tool emissions occur over a wide frequency range, at least from a few tens of hertz to around 10 kHz (Nedwell *et al.*, 1993). Whilst active sonar operates from a few kHz up to around 100 kHz, given the dimensions of the ear canal (roughly 2.5 cm long and with a diameter varying around 0.5 cm - Davis 1978) of particular interest recently are experiments involving the propagation of low frequency sound (from a few tens of hertz up to around 250 Hz) over long ranges (of order 1000 km) for climate monitoring. For detection over such long ranges, the sources of such sound are necessarily powerful (220 dB re 1 μPa at 1 m) (Baggeroer and Munk, 1992).

Comparatively little is known about air bubbles trapped within the ear canals of submerged humans, other than that they can occur. These bubbles are capable of having a significant effect on underwater hearing (Al Masri 1993). The precise geometry of these bubbles is not known, but the most likely shape is a cylindrical gas pocket, bounded at the curved wall by the flesh of the ear canal itself, and at the ends by the ear drum and the gas/water interface within the ear canal. The remainder of the canal would be water filled leading to the pinna, where a much larger body of water occurs external to the head. As with the column-cone model of the liquid body used in this investigation, the inertia of the oscillator will be invested primarily in the liquid contained within the ear canal, the radiation mass associated with the water outside of the head being far less significant, and the inertia of the entrained gas within the ear negligible. Therefore use of the simple linear theory given by equation 34 is justified for making estimations of the resonances (though clearly there is elasticity associated with the fleshy boundaries). Given typical ear canal dimensions, simple linear theory predicts that air bubbles trapped within divers' ears may be expected to resonate at such frequencies as those which, as outlined above, may occur at high intensity in the underwater environment. This is shown in figure 10, where the resonance for the piston-like motion of an ear canal, of 5 mm diameter and 2.5 cm length air-filled to 50%, 10% and 2%, are shown as a function of depth in both the adiabatic and isothermal limits. The increase in frequency of the piston-like mode with depth arises from the increase in ambient pressure. There will in addition be a resonance for the clamped-diaphragm model. Because of the relative gas volume changes which the two geometries can generate, it is likely that the piston-like motion can generate the larger pressure fluctuations within the gas.

The energetics of such resonances, and their harmonics, clearly may cause a noticeable effect within a system which is designed to be sensitive to acoustic stimulation through gas, rather than liquid, adjacent to the eardrum, and one might expect significant effects on the acoustics of the ear canal at these frequencies (from a few tens of hertz to a few hundred) if such bubbles were present. The mechanisms of underwater hearing itself are involved, and it is not a simple matter to theoretically extrapolate from this the effect of such bubbles on underwater hearing. However human diving is potentially hazardous, and the occurrence of any resonances coupling the human hearing, orientation and balance systems to an ocean medium which can contain intense sound at those frequencies must be considered.

There is far more documented evidence concerning the situations where one-dimensional bubbles might be expected to be exposed to high intensity acoustic fields.

The acoustic excitation of gas pockets which are stabilised within biological structures, the so-called "gas body activation" (Miller, 1984) was first considered to interpret the biological effects of ultrasound on the leaves of the aquatic plant *Elodea*, as discussed earlier (Miller, 1977). Such bodies have also been considered to discuss the mechanism of bioeffect when pockets of gas trapped in blood vessels, insect trachea and mammalian cells are subjected to ultrasonic irradiation.

There are conceivably many mechanisms of acoustic interaction with matter through which ultrasound could generate a bioeffect (ter Haar, 1986), and these potentially include both cavitational and non-cavitational ones. There are many possibilities through which cavitational bioeffects may potentially arise. If driven at low amplitude, the bubble will oscillate stably and repeatably, and such stable cavitation (of spherical bubbles) has been observed to cause bioeffect (Vivino *et al.*, 1985). However of particular concern has been the phenomenon of 'unstable' or 'transient' cavitation, typified in the explosive growth of unconfined spherical bubbles, followed by their rapid collapse. This collapse typically involves gas shocks and adiabatic heating of the gas to high temperature, both processes being capable of generating free radicals. The collapse is followed by a rebound, capable of generating liquid shocks. Transient cavitation being an almost instantaneous response to acoustic pressure changes, the presence or not of bubble activity during short-pulse regimes (such as lithotripter and diagnostic ultrasound) has been the object of much concern.

Damage resulting from exposure to lithotripter pulses *in vivo* often manifests in vessel walls, particularly in capillaries and medium-sized veins, with focal lesions in arterial walls tending to occur much less frequently (ter Haar *et al.*, 1994; Delius *et al.* 1990a, 1990b).The most sensitive organ to shock wave exposure is the lung, and Hartman (1990) demonstrated that fetal murine lung has a lower threshold for damage resulting from lithotripsy exposure than has the adult lung. This is presumed to be because of the absence of stabilised gas bodies within the fetal lung (ter Haar *et al.* 1994). Noting that Child *et al.* (1990) and Frizzell *et al.* (1994) have observed haemorrhage in mammalian lung resulting from exposure to pulsed ultrasound at levels low compared to those required to produce cavitation in tissues that do not contain stabilised gas bodies, ter Haar *et al.* (1994) comment that whilst the mechanism is not clear, it does appear to be mediated by existing stabilised gas bodies in tissue.

The question of whether cavitational effects are important, and what form they take, depends critically on the sound field which reaches the bubble, and upon the nature of that bubble. Attempts to understand cavitation bioeffects have been dominated by models of spherical bubbles (Leighton 1994), such that indications of the likelihood of

evoking an energetic response from a suitable free-floating microscopic spherical nucleus, should it exist, are characterised by a *mechanical index* (Holland and Apfel, 1989; Apfel and Holland 1991) which may be assigned to various operating conditions of clinical ultrasound devices. However the potential for bioeffects from a stabilised cylindrical bubble is another issue. As with spherical bubbles these may show the equivalent of not just 'stable', and 'transient', regimes. However if the gas bodies stabilised within biological structures resemble the one-dimensional bubbles discussed earlier in this paper, in certain circumstances it would be expected that the growth phase in transient behaviour is the key mechanism for bioeffect, in contrast to the traditional emphasis on the collapse phase in the transient cavitation of spherical bubbles.

Research has shown that if the medium resists bubble growth (for example, it is a liquid constrained to a fixed volume by structure, such a mammalian cell; or the gas pocket is itself part-bounded by rigid walls, for example the larval trachea), then stresses can be induced by the growth which may damage to the restraining structure (Ward *et al.*, 1983; Venter *et al.*, 1983; Aymé and Carstensen, 1989). However the analysis presented here shows that the bubble need not be surrounded by solid cell walls to exert significant stresses on the structure, if it is a within a tube-like structure.

The hypothesis to be examined here is that one-dimensional bubbles within lung capillaries may rupture the capillary during their growth phase. Consider how such gas pockets might arise. As blood flows away from the heart, it may be subjected to conditions which cause gas to come out of solution, including decompression or if the blood temperature were raised. Of particular note is the case of blood flowing in the pulmonary artery and subsequent branches. Conditions within the blood flowing from the heart to the lungs are designed to encourage gas to come out of solution. Whilst gas may transfer directly from the blood into the capillary wall, to the air-vesicle wall and from there to the air space, the conditions are such that gas may come out of solution within the blood itself (indeed, the interface between the blood and the vessel wall provides a suitable location for the nucleation of exsolution). Since the vessel size is continually decreasing, a bubble which with larger vessels grows to a size comparable with the capillary diameter may become trapped in position there. The exsolved gas contained within such vessels may in fact, as a result of the surface tension pressure, transfer more readily into the capillary wall which surrounds most of its volume than the gas which is still dissolved within the blood. The migration of gas-filled echo-contrast agents to blood vessels comparable with their size might also lead to this condition. In fact the bubble, no matter what its origin, need not even fill the cross-section of the vessel, since when subjected to tension by the ultrasonic pulse it will rapidly grow until its volume does fill a cross-section. It is at this point, no matter how

it comes about, that geometry of the one-dimensional bubble is attained and the key feature, that of the liquid inertia, comes into dominance.

This response of the one-dimensional bubble from this moment becomes radically different from that of the free-floating spherical bubbles normally considered, since the inertial term does not asymptotically tend to a finite value unless the enclosing tube widens significantly. For a pulsating spherical bubble of equilibrium radius R_O, the radiation mass has value $4\pi R_O^3\rho$ (Leighton, 1994). This has a finite and relatively small value because of the diverging geometry: if the meniscus velocity is $\dot{R}$ when the bubble has an instantaneous radius of R, then because of the spherically diverging geometry the liquid particle velocity at a distance r from the bubble centre is $\dot{r} = \dot{R}\,(R^2/r^2)$ (Minnaert, 1933). This inverse square law means that at large distances from the bubble, the liquid velocity is very small, so that the total kinetic energy invested in the liquid is finite, even within an infinite liquid medium. In contrast the liquid geometry in the one-dimensional bubble system shown in figure 1 clearly does not begin to diverge until the cone section, the inertial contribution from the liquid contained within the glass capillary tube increasing monotonically with the tube length. This can also been seen by examining the two contributing terms to the radiation mass for this system as given in equation 20: the inertia of the liquid in the pipe is $\rho A_O y_O$. In contrast to the spherical case, a one-dimensional bubble within an infinite non-diverging pipe would have infinite inertia, and so not be an oscillator at all. Therefore in the blood circulatory system, where the geometry does not simply and rapidly diverge but consists of long branching tubes, the inertia of such a bubble would be very high. On expansion, for example after the passage of a compressive pressure pulse or under a tension, the bubble cannot move the massive column of liquid within the blood system Since the liquid resists gross bubble growth, the stresses will be exerted on the capillary wall and the meniscus. If the stresses so exerted within the capillary wall are greater than the cohesion between the single layer of cells which make up the blood vessel wall, then haemorrhage will occur. The only other 'give' within the expanding one-dimensional bubble within the blood vessel is the meniscus: this will bow, causing local fluid motion and in the first instance, small gas volume change. If the deformation is sufficiently extreme daughter bubbles will be generated. However to do this a uniformly-bowing meniscus must pass through the hemispherical condition, where the surface tension pressure is a maximum. For a typical capillary of radius $\approx$10 μm this corresponds to a confining pressure of $\approx$30 kPa. Adhesion between capillary cells must exceed this to prevent haemorrhage. The ultimate tensile strength of the weakest tissue noted by Yamada (1973) is 50 kPa. Should daughter bubbles be in fact produced, these may seed further expansions, though still confined by the capillary. In summary, the

geometry acts against allowing the large-scale gas expansion required to relieve the stress on the capillary wall, and so prevent haemorrhage.

CONCLUSIONS

The dynamics of a one-dimensional bubble were developed, including a simple analysis of small-amplitude linear oscillations, analytical phase-space solutions of the undamped unforced equation of motion, and numerical solution to the full equation of motion. The theoretical results demonstrated the expected trends, and the analysis were capable of predicting the correct order for the oscillations of laboratory bubbles of centimetre-order length. With one-dimensional bubbles of such size, viscous effects are not negligible. The physical insights gained by the models allowed examination of the potentially biologically-significant cases of acoustic exposure of one-dimensional bubbles in divers' ear canals and within mammalian lung capillaries.

REFERENCES

Al Masri, M.A.O. 1993 Underwater Hearing Thresholds and Hearing Mechanisms, *University of Southampton, Ph.D. Thesis.*

Apfel, R.E., Holland, C.K. 1991 Gauging the likelihood of cavitation from short-pulse, low-duty cycle diagnostic ultrasound. *Ultrasound in Med. & Biol.* **17** 179-185.

Aymé, E.J., Carstensen, E.L. 1989a Cavitation induced by asymmetric distorted pulses of ultrasound: Theoretical Predictions. *IEEE Trans. on Ultrasonics, Ferroelectrics and Frequency Control* **36** 32-40.

Baggeroer, A. and Munk, W. 1992 The Heard Island Feasibility Test. *Physics Today,* **45** 22-30.

Child, S.Z., Hartman, C.L., Schery, L.A. and Carstensen, E.L. 1990 Lung damage from exposure to pulsed ultrasound. *Ultrasound Med. Biol.* **16** 817.

Davis H. 1978 Anatomy and Physiology of the Auditory System. Chapter 3 in: *Hearing and Deafness* , Davis H. and Silverman S.R. ©1947 Holt, Rinehart and Winston (New York, London). 4th Edition, 1978.

Delius M., Jordan M., Liebich H.-G., Brendel W. 1990a Biological effects of shock waves: Effect of shock waves on the liver and gallbladder wall of dogs - Administration rate dependence. *Ultrasound Med. Biol.* **16** 459-466.

Delius, M., Denk, R., Berding, C., Liebich, H., Jordan, M., Brendel, W. 1990b Biological effects of shock waves: cavitation by shock wave in piglet liver. *Ultrasound Med. Biol.* **16** 467-472.

Devin, C. Jr. 1959 Survey of Thermal, Radiation, and Viscous Damping of Pulsating Air Bubbles in Water. *J. Acoust. Soc. Am.* **31** 1654.

Forsythe, G.E., Malcom, M.A. and Moler, L.B. 1977 Computer Methods for Mathematical Computations. Prentice-Hall.

French, A.P. 1979 Vibrations and Waves. Nelson, London.

Frizzell, L.A., Chen, E and Lee, C. 1994 Effects of pulsed ultrasound on the mouse neonate: hind limb paralysis and lung haemorrhage. *Ultrasound Med. Biol.* **20.**

Hartman, C., Child, S.Z., Mayer, R., Schenk, E., Carstensen, E.L. 1990 Lung damage from exposure to the fields of an electrohydraulic lithotripter. *Ultrasound Med. Biol.* **16** 675-679.

Holland C.K., Apfel R.E. 1989 An improved theory for the prediction of microcavitation thresholds. *IEEE transactions on ultrasonics, Ferroelectrics, and Frequency Control* **36** 204-208.

Howkins, S.D. 1965 Measurements of the resonant frequency of a bubble near a rigid boundary. *J. Acoust. Soc. Am.* **37** 504-508.

Leighton, T.G. 1994 The Acoustic Bubble. *Academic Press, London.*

Miller, D.L. 1977 The effects of ultrasonic activation of gas bodies in *Elodea* leaves during continuous and pulsed irradiation at 1 MHz. *Ultrasound in Med. Biol.* **3** 221-240.

Miller, D.L. 1979 A cylindrical bubble model for the response of plant-tissue gas-bodies to ultrasound. *J. Acoust. Soc. Am.* **65** 1313-1321.

Miller, D.L. 1984 Gas body activation. *Ultrasonics* **22** 261-269.

Miller, D.L., Nyborg, W.L. 1983. Theoretical explanation of the response of gas-filled micropores and cavitation nuclei to ultrasound. *J. Acoust. Soc. Am.* **73** 1537-1544.

Miller, D.L., Neppiras E.A. 1985 On the oscillation mode of gas-filled micropores. *J. Acoust. Soc. Am.* **77** 946-953.

Minnaert, M. 1933 On musical air-bubbles and sounds of running water, *Phil. Mag.* **16** 235-248.

Molvaer, O.I. and Gjestland, T. 1981 Hearing damage risk to divers operating noisy tools underwater. *Scan. J. Work Environ. Health* **7** 263-270.

Nedwell, J.R., Martin, A.M. and Mansfield, N. 1993 Underwater tool noise: Implications for hearing loss. In: Advances in Underwater Technology, Ocean Science and Offshore Engineering. *Society for Underwater Technology, Kluwer Academic Publishers, Netherlands.* **31** 267-275.

ter Haar, G.R. 1986 Therapeutic and surgical applications. In*: Physical principles of Medical Ultrasonics.* Hill CR, ed. Ellis Harwood Ltd, Chichester (for John Wiley and Sons, New York). Part III: Biophysical implications and applications.

ter Haar, G.R., Frizzell, L.A., Delius, M. and Stratmeyer, M. 1994 Non-thermal bio-effects: Organs, Cells, Tissues. Chapter 5 of: *WFUMB Symposium on Safety of Ultrasound in Medicine: Emphasis on non-thermal mechanisms* (Draft Document, Utsunomiya, Japan, 11-15 July 1994).

Venter, R.D., Ward, C.A., Ho, S., Johnson, W.R., Fraser, W.D., Landolt, J.P. 1983 Fracture studies on mammalian semicircular canal. *Undersea Biomed. Res.* **10** 225-240.

Vivino, A.A., Boraker, D.K., Miller, D., Nyborg, W. 1985 Stable cavitation at low ultrasonic intensities induces cell death and inhibits ^{3}H-TdR incorporation by con-a-stimulated murine lymphocytes *in vitro. Ultrasound in Med. & Biol.* **11** 751-759.

Ward, C.A., Johnson, W.R., Venter, R.D., Ho, S., Forest, T.W., Fraser, W.D. 1983 Heterogeneous bubble nucleation and conditions for growth in a liquid-gas system of constant mass and volume. *J. Appl. Phys.* **54** 1833-1843.

Yamada, H. 1973. Strength of Biological Materials (Evans, F.G., ed.). Krieger, New York.

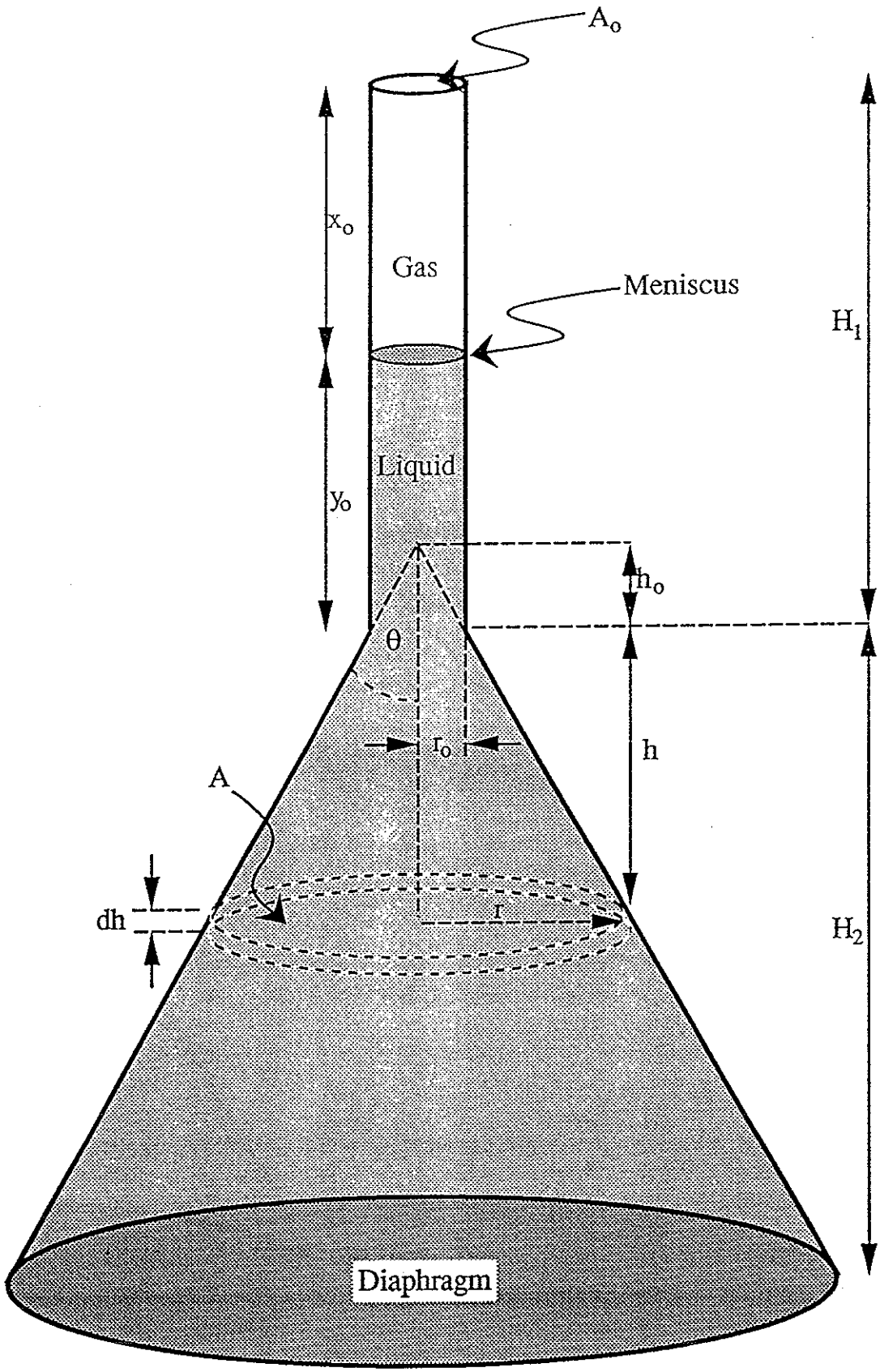

Figure 1

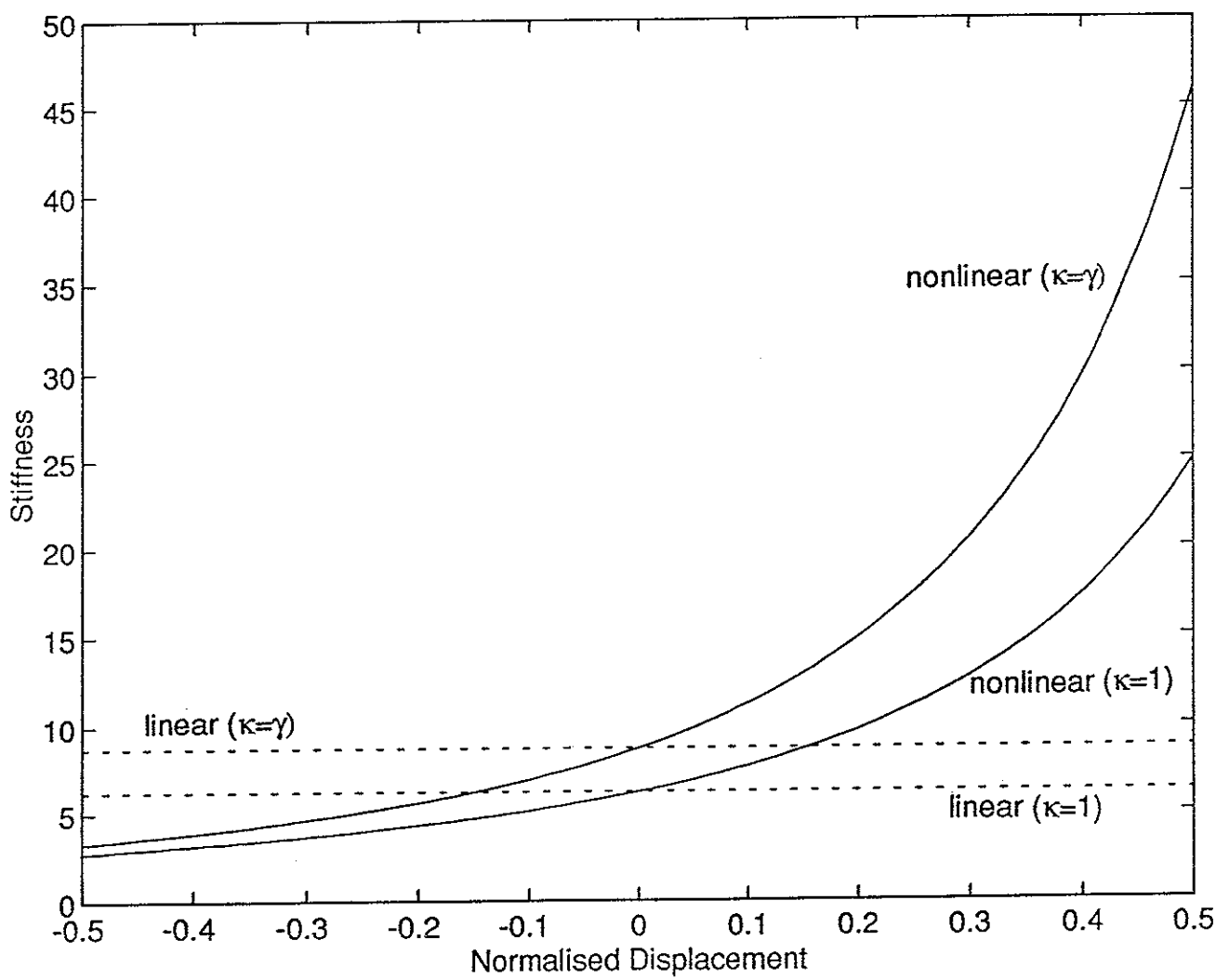
50
45
40
35
30
25
20
15
10
5
0
Stiffness
-0.5
-0.4
-0.3
-0.2
-0.1
0
0.1
0.2
0.3
0.4
0.5
Normalised Displacement
nonlinear (κ=γ)
nonlinear (κ=1)
linear (κ=γ)
linear (κ=1)

Figure 2

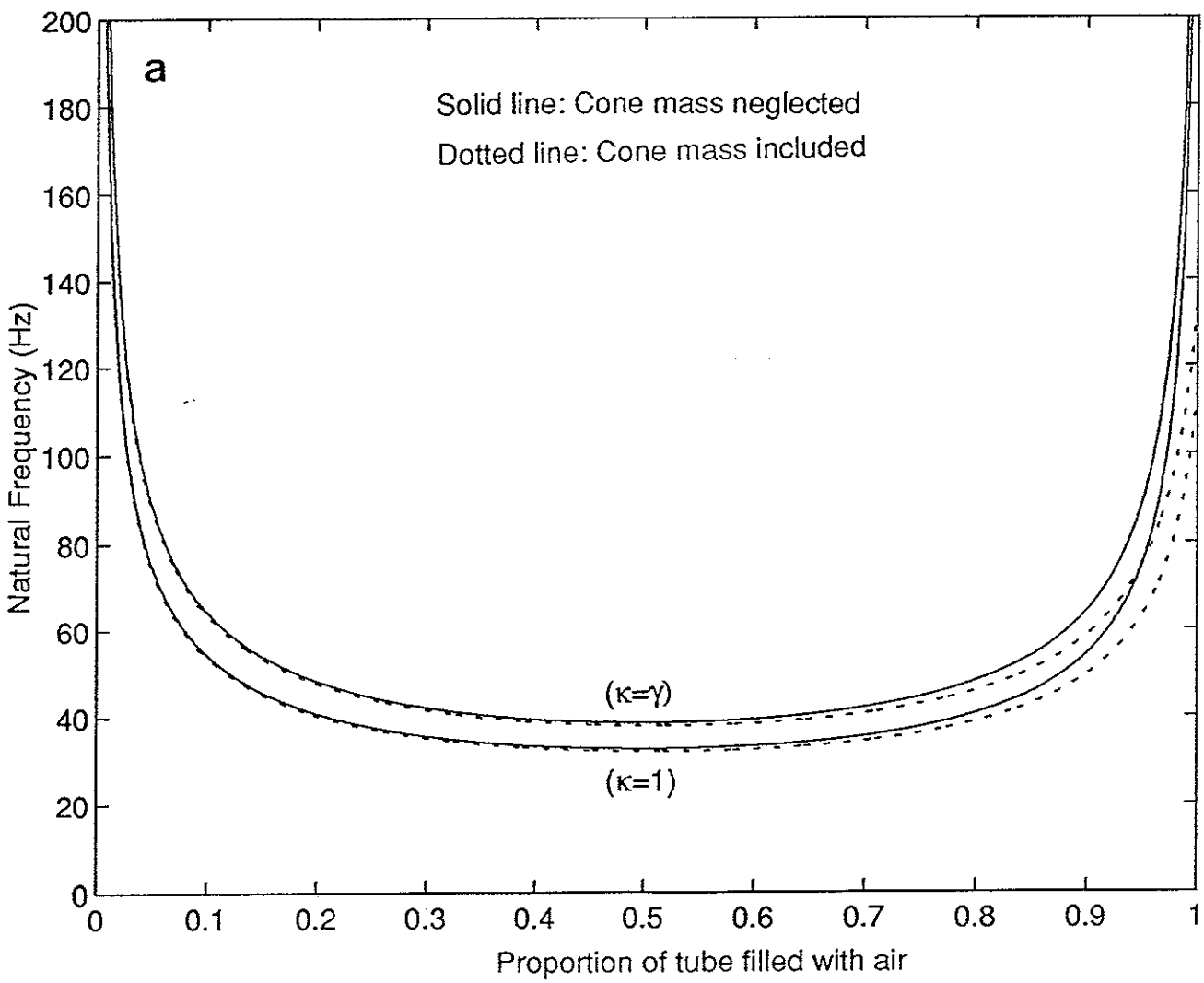
a
Solid line: Cone mass neglected
Dotted line: Cone mass included
(κ=γ)
(κ=1)
Natural Frequency (Hz)
Proportion of tube filled with air
0
20
40
60
80
100
120
140
160
180
200
0
0.1
0.2
0.3
0.4
0.5
0.6
0.7
0.8
0.9
1

Figure 3a

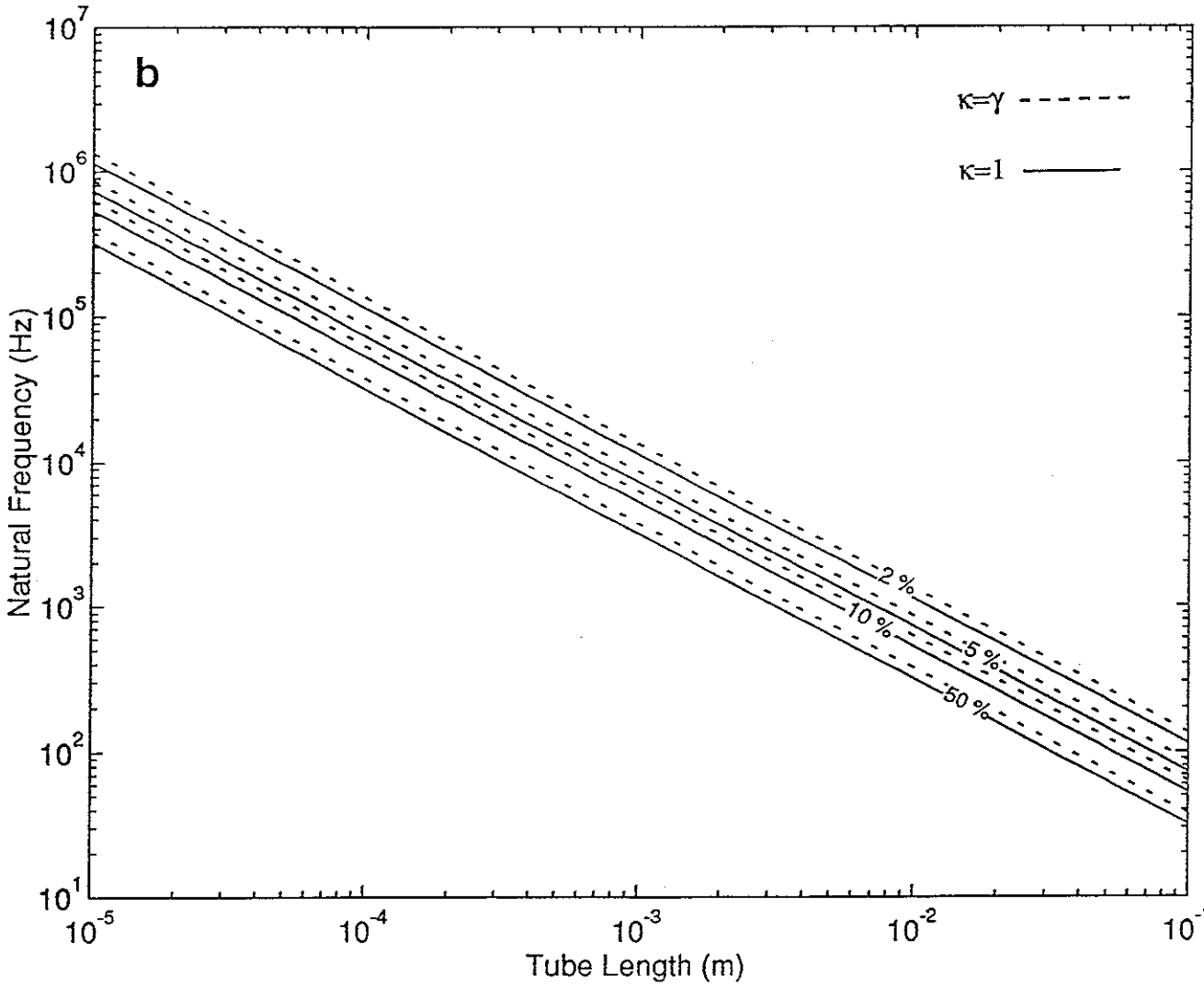
b
κ=γ
κ=1
2 %
5 %
10 %
50 %
Natural Frequency (Hz)
Tube Length (m)
10^7
10^6
10^5
10^4
10^3
10^2
10^1
10^-5
10^-4
10^-3
10^-2
10^-1

Figure 3b

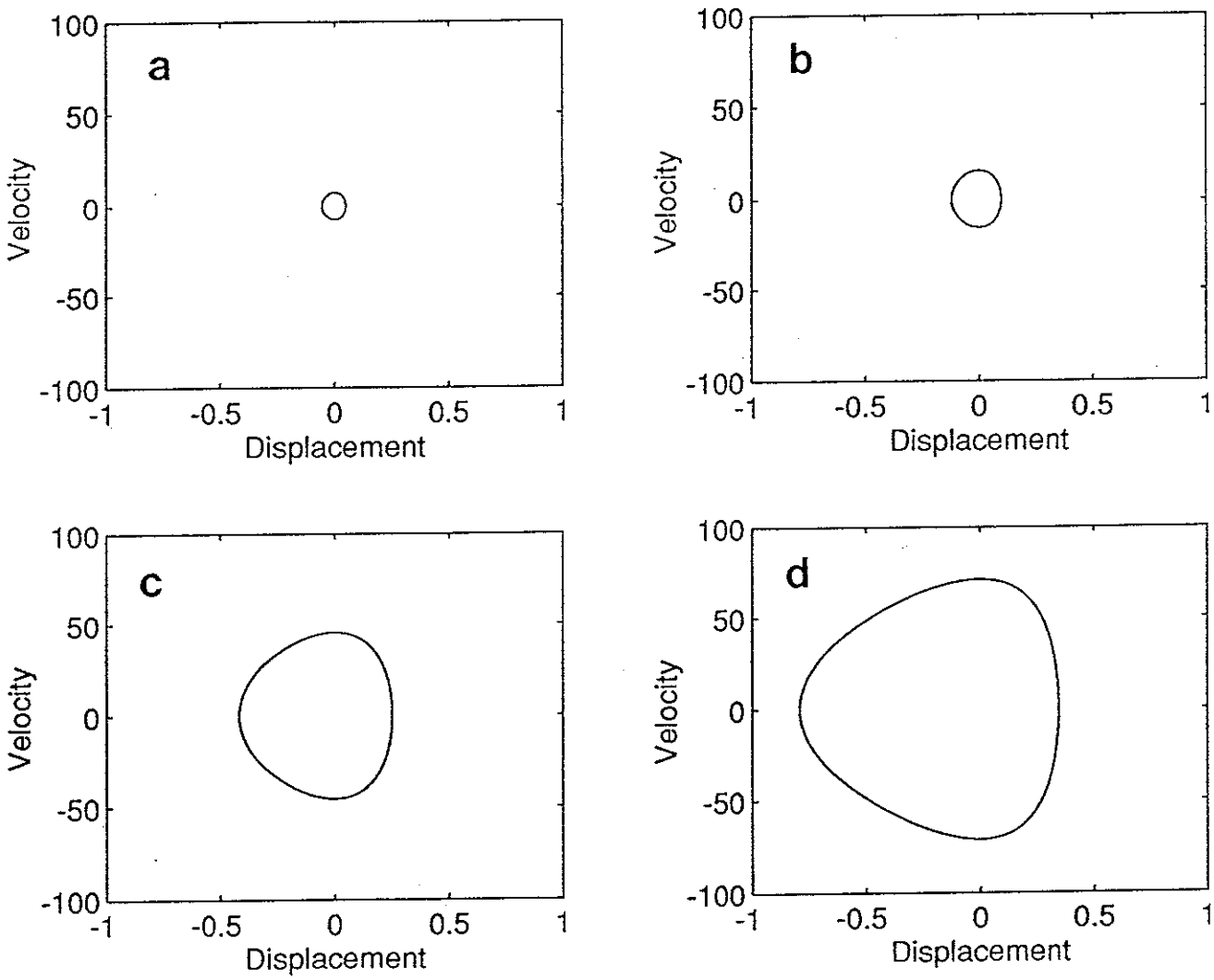

Figure 4

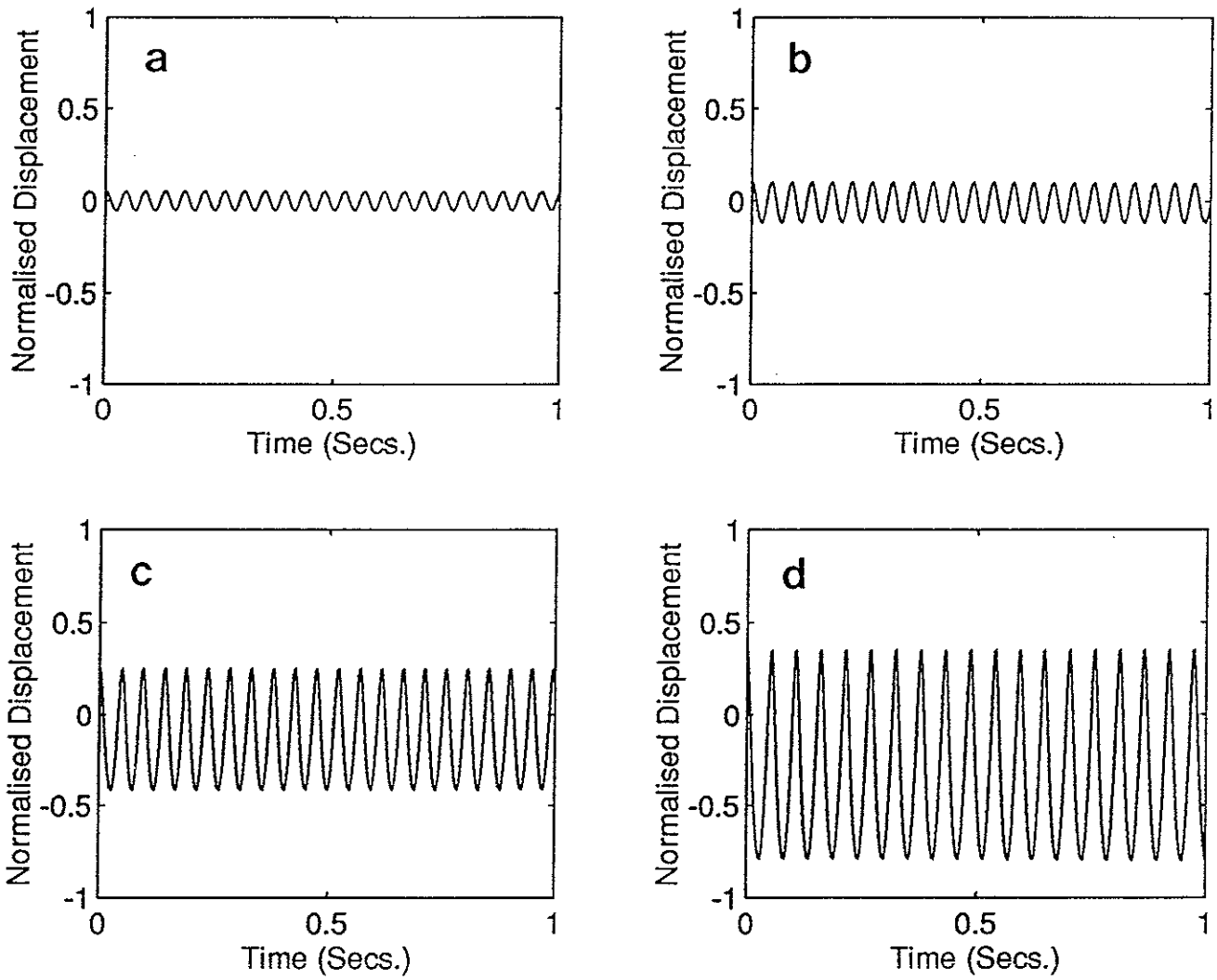

Figure 5

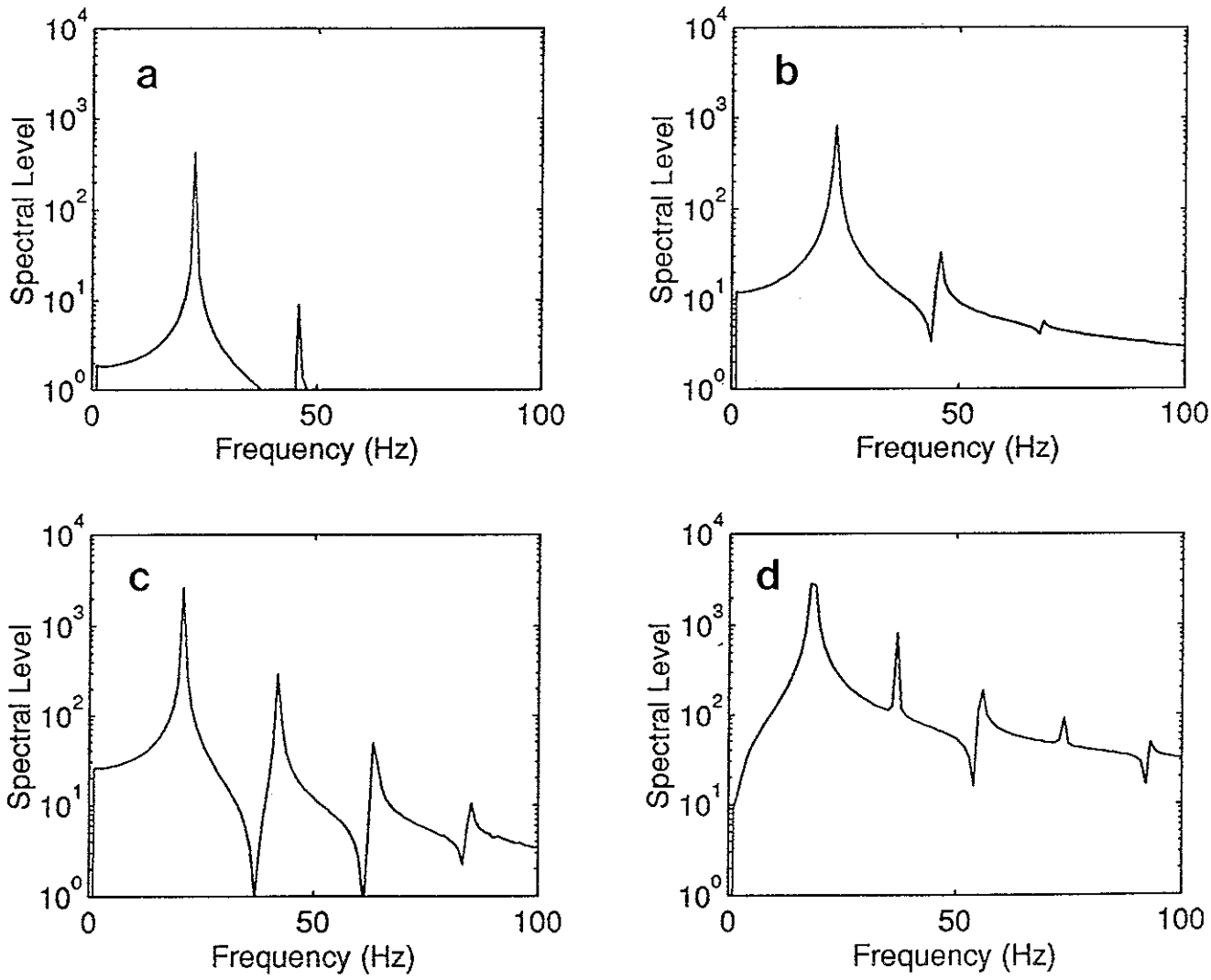

Figure 6

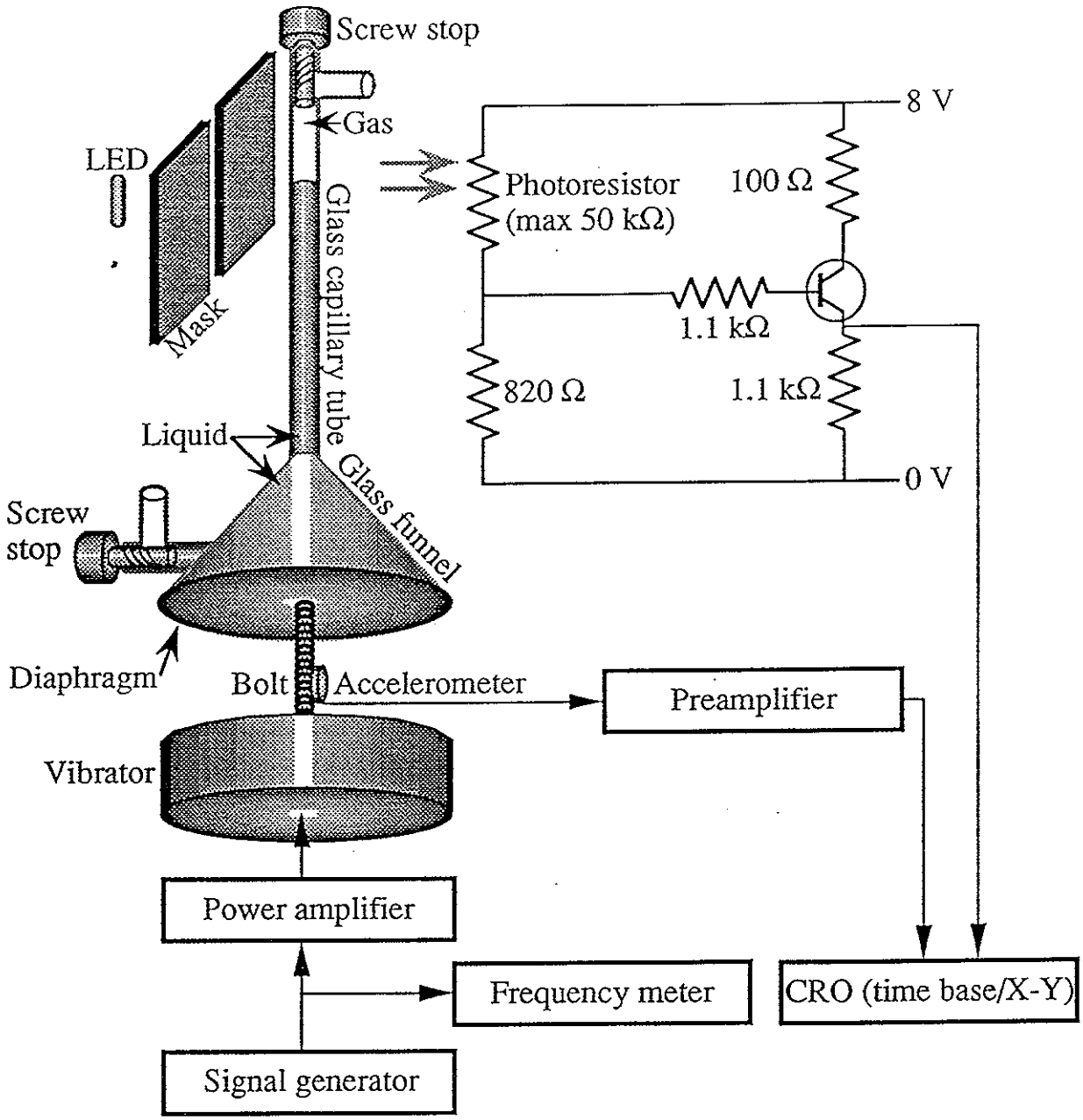
Screw stop
Gas
LED
Mask
Glass capillary tube
Photoresistor
(max 50 kΩ)
8 V
100 Ω
1.1 kΩ
820 Ω
1.1 kΩ
0 V
Liquid
Glass funnel
Screw
stop
Diaphragm
Bolt
Accelerometer
Preamplifier
Vibrator
Power amplifier
Frequency meter
CRO (time base/X-Y)
Signal generator

Figure 7

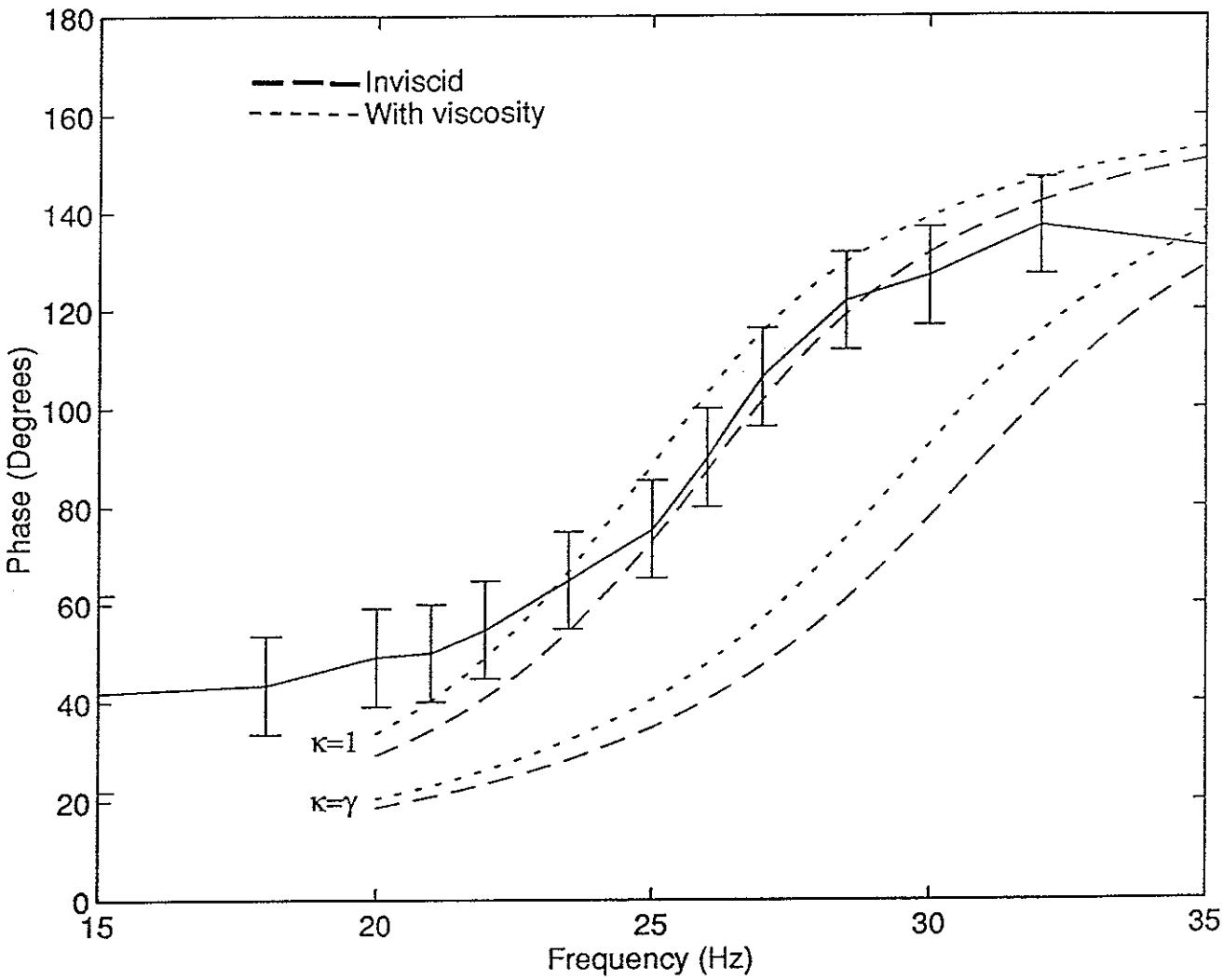
Inviscid
With viscosity
κ=1
κ=γ
Phase (Degrees)
Frequency (Hz)
180
160
140
120
100
80
60
40
20
0
15
20
25
30
35

Figure 8

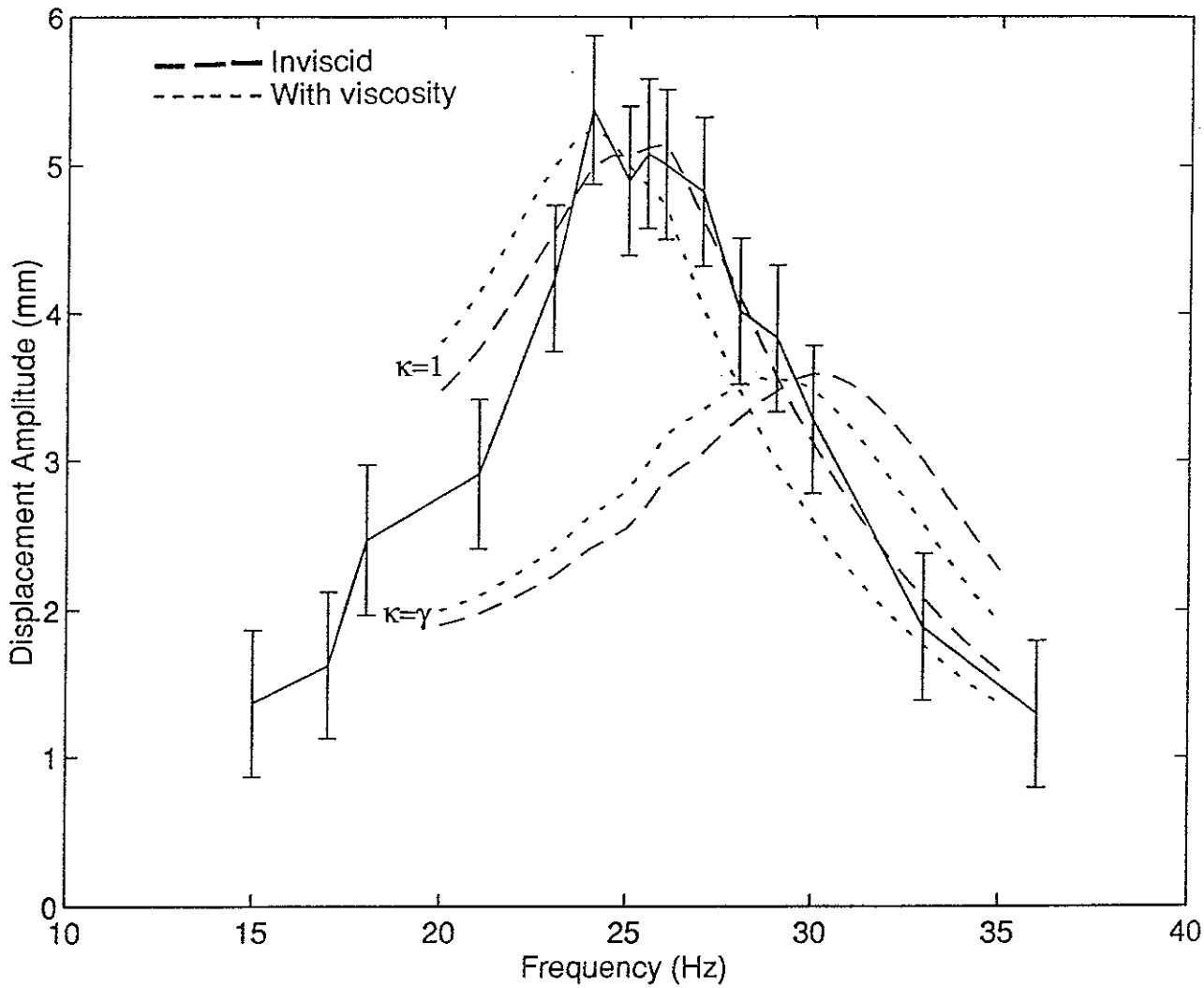
Inviscid
With viscosity
κ=1
κ=γ
Displacement Amplitude (mm)
Frequency (Hz)
0
1
2
3
4
5
6
10
15
20
25
30
35
40

Figure 9a

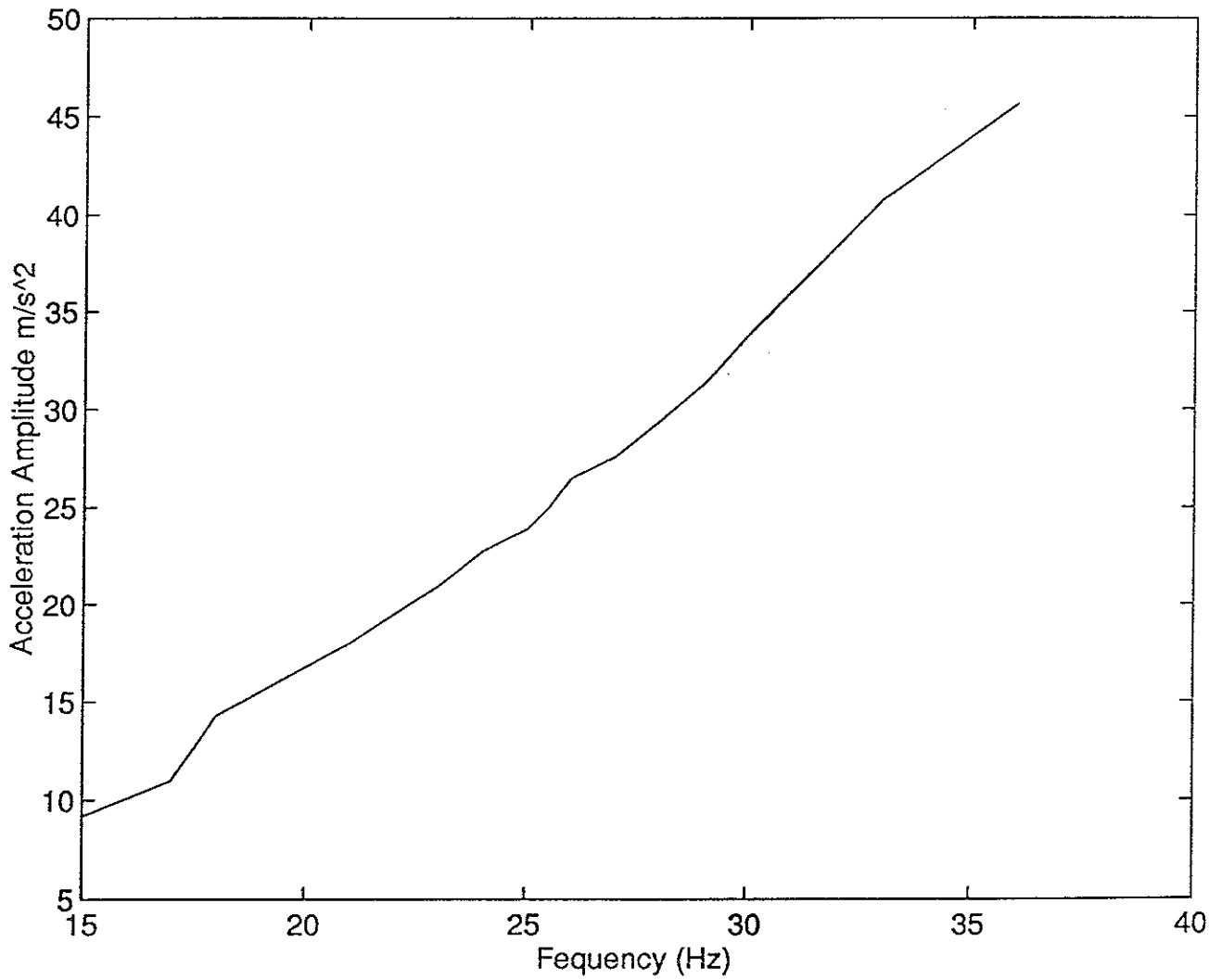
Acceleration Amplitude m/s^2
Fequency (Hz)
50
45
40
35
30
25
20
15
10
5
15
20
25
30
35
40

Figure 9b

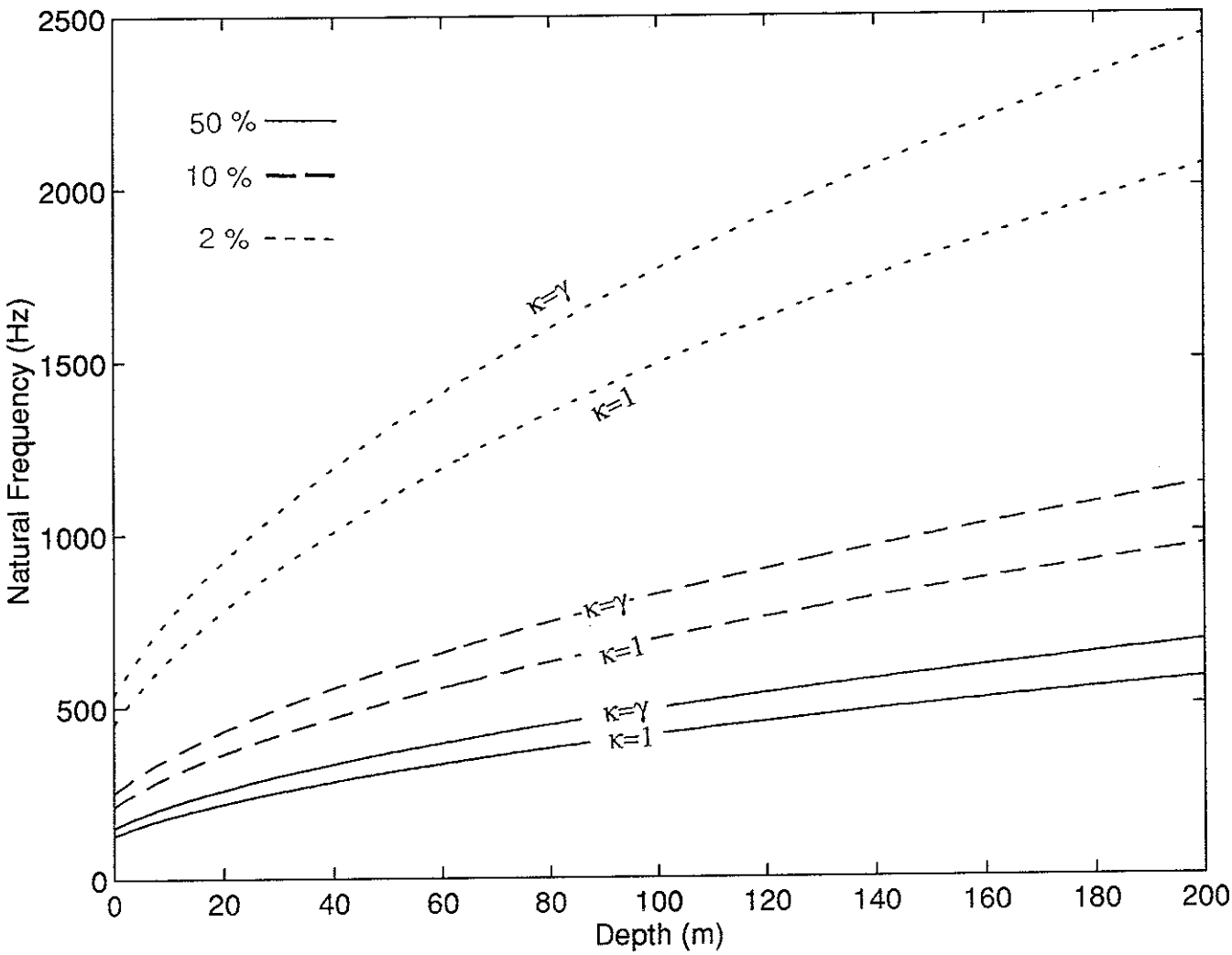
2500
2000
1500
1000
500
0
Natural Frequency (Hz)
0
20
40
60
80
100
120
140
160
180
200
Depth (m)
50 %
10 %
2 %
κ=γ
κ=1
κ=γ
κ=1
κ=γ
κ=1

Figure 10